Diagenetic sequences of continuously deposited tight sandstones in various environments: A case study from upper Paleozoic sandstones in the Linxing area, eastern Ordos basin, China

Yong Li, Xiangdong Gao, Shangzhi Meng, Peng Wu, Xinlei Niu, Peng Qiao, and Derek Elsworth

ABSTRACT

An integrated analysis of the petrographic characteristics and types and distribution of diagenetic alteration in the upper Paleozoic Benxi–Taiyuan, Shanxi, and Xiashihezi Formations provides insights into the controlling factors on variations in porosity and permeability in tight sandstones (85% of the sandstone samples display porosity values <10% and 90% of the samples exhibit permeability <1 md).

Diagenetic alteration includes mesogenetic compaction, cementation by dolomite, ankerite, and quartz, dissolution of feldspar, and illitization of smectite. Eodiagenesis includes compaction, development of smectite, cementation by pore-filling quartz and disordered kaolinite, and precipitation of calcite and Fe-calcite. Chlorite and quartz preserve primary pores against damage, whereas kaolinite, illite–smectite (I/S) mixed layer, and illite significantly diminish reservoir quality via permeability reduction. Chlorite and I/S content decrease abruptly as depth increases, whereas the kaolinite content remains elevated at depth because of the complete destruction of K-feldspar. The transformation from smectite to illite provides silica ions for the widely distributed quartz overgrowths. As the depositional environment transformed from fluvial (Xiashihezi) to deltaic

Manuscript received March 21, 2018; provisional acceptance June 5, 2018; revised manuscript received July 27, 2018; revised manuscript provisional acceptance October 10, 2018; 2nd revised manuscript received November 4, 2018; 2nd revised manuscript provisional acceptance December 10, 2018; 3rd revised manuscript received December 18, 2018; final acceptance March 6, 2019.
DOI:10.1306/03061918062

AUTHORS

YONG LI ~ *State Key Laboratory of Coal Resources and Safe Mining and College of Geosciences and Surveying Engineering, China University of Mining and Technology, Beijing, People's Republic of China; Shandong Provincial Key Laboratory of Depositional Mineralization and Sedimentary Minerals, Shandong University of Science and Technology, Qingdao, Shandong, People's Republic of China; liyong@cumtb.edu.cn*

Yong Li is an associate professor in petroleum and natural gas geology. His interests are in the areas of sedimentology, reservoir characterization, and issues associated with unconventional hydrocarbons, including coalbed methane, tight gas, shale gas, and gas hydrate. He is the corresponding author of this paper.

XIANGDONG GAO ~ *State Key Laboratory of Coal Resources and Safe Mining and College of Geosciences and Surveying Engineering, China University of Mining and Technology, Beijing, People's Republic of China; gaoxd1990@163.com*

Xiangdong Gao is a Ph.D. candidate in petroleum geology researching gas shale, coalbed methane, and tight sandstone reservoirs.

SHANGZHI MENG ~ *China United Coalbed Methane Corp., Ltd., Beijing, People's Republic of China; mszlily@126.com*

Shangzhi Meng is a senior engineer at China United Coalbed Methane Corp., Ltd. His interests are in the areas of deep coalbed methane extraction and coal measure gases production.

PENG WU ~ *China United Coalbed Methane Corp., Ltd., Beijing, People's Republic of China; wupeng19@cnooc.com.cn*

Peng Wu is an engineer at China United Coalbed Methane Corp., Ltd. His interests are in the fields of sedimentology, tight gas, and coalbed methane reservoir evaluation and production.

XINLEI NIU ~ *State Key Laboratory of Coal Resources and Safe Mining and College of*

Geosciences and Surveying Engineering, China University of Mining and Technology, Beijing, People's Republic of China; 1668525686@qq.com

Xinlei Niu is a master in coal geology, researching gas shale, coalbed methane, and tight sandstone reservoirs.

PENG QIAO ~ *State Key Laboratory of Coal Resources and Safe Mining and College of Geosciences and Surveying Engineering, China University of Mining and Technology, Beijing, People's Republic of China; 836815612@qq.com*

Peng Qiao is a Ph.D. candidate at the University of Chinese Academy of Sciences and graduated from China University of Mining and Technology, Beijing. His interests are in the field of shale gas, coalbed methane, and tight sandstone reservoirs.

DEREK ELSWORTH ~ *Departments of Energy and Mineral Engineering and Geosciences, Earth and Mineral Sciences Energy Institute, Center for Geomechanics, Geofluids, and Geohazards (G3), Pennsylvania State University, University Park, State College, Pennsylvania; elsworth@psu.edu*

Derek Elsworth is a professor at the G3 Center at Pennsylvania State University. His interests are in the areas of computational mechanics, rock mechanics, and in the mechanical and transport characteristics of fractured rocks and unconventional hydrocarbons, including coal gas, tight gas shales, and hydrates.

ACKNOWLEDGMENTS

We would like to thank AAPG Editor Barry J. Katz for his careful revisions and great suggestions in improving the manuscript. This research was financially supported by the Natural Science Foundation of China (grant 41702171), Beijing Municipal Excellent Talents Foundation (2017000020124G107), 2017 Open Project Fund of State Key Laboratory of Coal Resources and Safe Mining (SKLCRSM17KFA12). We also thank China United Coalbed Methane Corp., Ltd., for providing convenient access to the field work and well test reports.

(Shanxi) and to epicontinental (Taiyuan and Benxi), the dissolution effect increased monotonically. Feldspar dissolution is dominant in the Shanxi Formation, whereas the Benxi and Taiyuan Formations commonly contain quartz dissolution pores. The Taiyuan Formation has markedly higher porosities than in the overlying and underlying formations, caused by strong dissolution and high silica content. The decrease in porosity in the Benxi Formation results from the extensive formation of clay minerals caused by high frequency transgressions in a transitional environment.

INTRODUCTION

The late Carboniferous to early Permian is characterized in northern China by the presence of extensive coal deposits and associated coalbed methane accumulations (Tang et al., 2004; D. Liu et al., 2009; Yao et al., 2009; Li et al., 2017b, 2019). This interval is largely represented by the Benxi, Taiyuan, Shanxi, and Xiashihezi Formations (chronological order from base to top) that were deposited in an epicontinental shelf to delta and fluvial environment (Li et al., 2016). In recent decades, tight gas reservoirs have been widely developed in the Ordos basin, with successful development in the lower Permian Xiashihezi Formation in the Sulige, Yulin, Daniudi, and Jingbian fields (Zhang et al., 2009; Zou et al., 2013). With the recent discovery of substantial gas reserves and attainable high production demonstrated in sandstones interbedded with coal seams, it is important to define the characteristic petrographic and petrophysical features that support prolific production in these low-permeability sandstones. Analyzing and comparing different depositional environments, compositions, and diagenetic and other features among the formations enables the factors that control reservoir quality of the Ordos basin to be defined. The release of organic acids and CO_2 during the coalification and maturation process of organic matter can influence the distribution of clay minerals and the overall diagenetic evolution of a sandstone (Van Keer et al., 1998; Shuai et al., 2013). As for the eastern Ordos basin, coal seams occur with sandstones deposited in their overlying or underlying strata (Li et al., 2017a). Thus, these results may be referenced both to and among other tight gas reservoirs interbedded with coal-bearing strata to further define and reinforce key characteristics that indicate prolific production.

Tight sandstone reservoirs generally experience complex diagenetic histories that progressively changed reservoir quality (Karim et al., 2010; Zhang et al., 2015; Hansen et al., 2017; Lai et al., 2017). Reservoir quality is controlled by detrital composition, depositional environment, sedimentary facies, burial temperature, pressure, and chemical composition of the pore water (Taylor et al., 2010; Bjørlykke, 2014). The linkage of

diagenesis to diagenetic structure and transport properties is complex but includes the (1) effects of mechanical compaction during burial history (Taylor et al., 2010); (2) chemical processes of mineralogical conversions (Karim et al., 2010; Stroker et al., 2013); (3) sources of cements and sinks of chemical components (Bjørlykke and Jahren, 2012); (4) fluid chemistry, temperature, and stress experienced during evolution (Macaulay et al., 1993; Liu et al., 2014); and (5) impact of depositional facies and sequence stratigraphy on diagenetic minerals and their transformations, especially in coastal or deltaic environments (Morad et al., 2000; El-ghali et al., 2006, Karim et al., 2010; D. Lv et al., 2017). Despite, or maybe because of, this long list, many uncertainties remain in associating these mechanisms with a quantitative analysis of the mass transfer process and their significance in predicting reservoir quality (Yasuhara et al., 2003; Gier et al., 2008; Bjørlykke, 2014).

A series of petrographic and geochemical studies have reported on the gas and oil accumulation features of the Yanchang (mainly the Chang 7 Member) in the Triassic and the Xiashihezi (mainly He 8 Member) Formations in the Permian of the Ordos basin (Yuan et al., 2015; Ma et al., 2018). However, fewer observations and studies constrain the Benxi, Taiyuan, and Shanxi Formations despite recent reports of their huge gas potential (Li et al., 2017a). To better understand the key factors controlling reservoir quality (storage and delivery properties), the primary objectives of the investigation are threefold: (1) to investigate the diagenetic process of sandstones from the Benxi–Taiyuan (deposited in epicontinental environment), Shanxi (fluvial-deltaic environment), and Xiashihezi Formations (fluvial environment); (2) to evaluate the factors controlling compaction, cementation, and dissolution processes that affect reservoir quality; and (3) to reconstruct the diagenetic history while highlighting the key factors controlling the storage and delivery properties of the sandstones. The results mainly focus on the mass balance and mineral alterations influenced by different sedimentary environments and their controls on reservoir characteristics. Furthermore, the diagenetic controls of sandstones interbedded within coal seams, characterized by the frequently fluctuating sedimentary environment, are also discussed, defining a range of issues that must be resolved so that index characteristics may be robustly defined to aid in the prospecting of prolific gas reservoirs from these environments.

GEOLOGICAL SETTING

The Ordos basin is a large intracontinental basin located in the central part of the North China plate and is subdivided into six structural units (the Yimeng uplift, Jinxi fold, Weibei uplift, Western thrusted zone, Tianhuan sag, and Yishan slope) (Ji et al., 2010; Yang et al., 2017). The study area is located in the Jinxi fold in the eastern part of the Ordos basin (Figure 1). The strata generally strike north to south and dip to the west as a smooth monocline at angles of 3° to 10° that decrease to less than 1° upon entering the main part of the basin (Li et al., 2017b).

The Ordos basin was an intraplate remnant cratonic basin during the Triassic to Early Cretaceous (Lai et al., 2016). During the Cambrian–Early Ordovician and Middle Ordovician–Middle Triassic, the basin changed from a cratonic basin with divergent margins to one with convergent margins (Yang et al., 2005; C. Liu et al., 2009). The structures occurring around the basin generally developed during the late Yanshanian orogeny (ca. 130–90 Ma) as the whole basin was uplifted, and the east margin was uplifted more intensively than the remainder (Gao et al., 2000; Wang et al., 2008).

The upper Carboniferous sequence developed directly upon the dolomitic limestone of the Middle Ordovician, with a hiatus and ensuing erosion occurring during the Late Ordovician to early Carboniferous (Yang et al., 2005). Two sets of source rocks are widely developed in the study area, comprising thick-bedded coal and dark-colored mudstones in the Taiyuan and Shanxi Formations (Zhang et al., 2009). The coal and mudstones are rich in organic matter, with a thermal maturity of approximately 1.4% vitrinite reflectance and with type II_2 to III kerogens in the Linxing area (Li et al., 2016). The coal thicknesses range from 8 to 18 m (26 to 59 ft) and 4 to 14 m (13 to 50 ft) in the Taiyuan and Shanxi Formations, respectively. Sandstone bodies are interpreted as tidal bars and distributary channel deposits in the Taiyuan Formation and fluvial and distributary channel deposits in the Shanxi and Xiashihezi Formations (Liu et al., 2016; N. Xu et al., 2017).

Tight gas reservoirs are developed in the Benxi, Taiyuan, Shanxi, and Xiashihezi Formations (Figure 2). The Benxi and Taiyuan Formations were deposited in an epicontinental environment, with rapid sea-level changes occurring on four occasions because of rapid transgressions and slow regressions (Li et al., 2015). The Shanxi Formation was deposited in a deltaic environment with well-developed, thick coal seams (Ren et al., 2014). During the deposition of the Xiashihezi Formation, the sea had completely regressed from northern China, and the study area was dominated by a fluvial environment with thick fluvial sandstone bodies (Figure 2). Large volumes of gas were generated during the Jurassic as the source rocks in the upper Paleozoic strata became mature in the Early Jurassic and peak gas generation occurred at the end of the Late Jurassic (Zhao et al., 2012). Furthermore, another stage of gas generation occurred during the middle Cretaceous as magmatic activity occurred in the southeastern part of the Linxing area where the Zijinshan pluton was intruded (Figure 3; Li et al., 2016).

SAMPLES AND METHODOLOGY

Drill cores, well logs, and borehole geochemical and geophysical test data were obtained from many of the exploration wells in the study area. The samples used in this study were obtained from wells over sampling depth intervals of 1200–2200 m (3937–7218 ft). A total of 404 samples were used from the main sandstones from the Benxi, Taiyuan, and

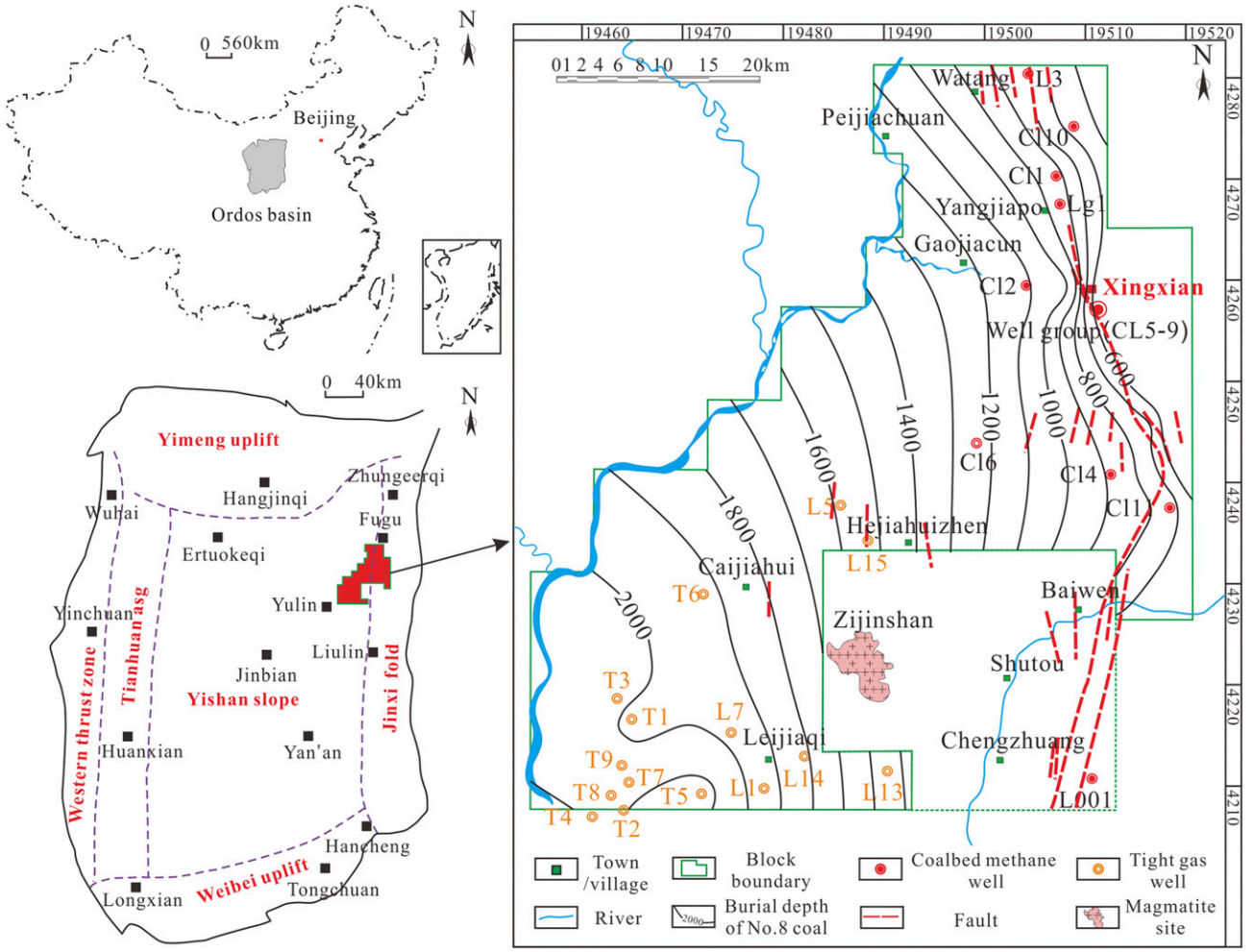

Figure 1. Location of the Linxing area, northeastern Ordos basin; the right part shows the burial depth of the no. 8 coal seams in the Taiyuan Formation. C, CL, L, and T are the names of wells.

Shanxi Formations as recovered from 15 gas wells in the tight sandstones (Figure 1).

More than 250 observations from thin sections and measurements of reservoir porosity and permeability, scanning electronic microscopy (SEM) analyses, and corresponding well-log data were collected from the China United Coalbed Methane Corp., Ltd. The SEM observation was carried out with the ZEISS EVO MA 15 after the SY/T 5162-1997. All the samples were plated gold and measured at 25°C and 50% humidity, which was used to identify the detrital grains, clay minerals, and different pores. The cylindrical core plugs, with diameter of 25 mm (0.98 in.) and length of 50 mm (1.97 in.), were adopted for measuring the porosity and permeability. The porosity and permeability were tested on an AP-608 automated permeameter–porosimeter with helium (Adebayo et al., 2017).

Rock mineralogies and visual pore structures were analyzed using polished thin sections impregnated with colored epoxy to better define diagenetic processes. Mineralogy was quantified by point counting minerals using approximately 200 points per sample as well as by employing thin-section porosity. The maximum counting errors varied with the percentages of the constituents from ±3.6% at 50% content to ±2.1% at 10% content (Folk, 1974). The volumetric mineralogical contents of the rock constituents, such as calcite and quartz cements, as well as pores were measured from the photomicrographs of thin sections using an Olympus microscope equipped with a CL8200-MKS CL attachment following the method of Wang et al. (2015). In addition, grain size and sorting were also determined by measurements of at least 120 grains per thin section. We conducted x-ray diffraction (XRD) analysis using a Rigaku D/MAX-2500 V/PC powder diffractometer equipped with Ni-filtered Cu-Kα radiation and scintillation detector, with the mineral phase evaluated by Clayquan software (version 2016). Fluid inclusions were mainly collected from quartz overgrowths and fractures inside quartz in sandstones of the Benxi, Taiyuan, Shanxi, and Xiashihezi Formations to obtain the temperature of homogenization and salinity. All samples were measured with a Linkam THMS600 at 20°C and 30% humidity, with the method referenced in Z. Xu et al. (2017).

RESULTS

Sandstone Composition

Petrographic investigation showed that the sandstones are litharenites, feldspathic litharenites, lithic arkoses, and sublitharenites. The Xiashihezi Formation is dominated by feldspathic litharenites (75% by whole-rock volume), followed by litharenites (23%) with a few lithic arkoses. The Shanxi Formation is mainly composed of feldspathic litharenites (57%) and litharenites (35%), with a few lithic arkoses and sublitharenites. The Taiyuan Formation is dominated by litharenites (73%) and includes 22% feldspathic litharenites and almost 5% quartzarenites. The Benxi Formation sandstones can be classified as litharenites (36%) and sublitharenites (35%) with a significant amount of feldspathic litharenites (24%) (Figure 4; Table 1).

The detrital components comprise approximately 45%–65% quartz, which is the most abundant detrital mineral. The quartz content increases slightly from the Xiashihezi Formation to the Benxi Formation as the sedimentary environment transited from a fluvial delta to an epicontinental environment (Li et al., 2015). The average chert volume is high in the Benxi Formation, with an average value of 2.1%. Plagioclase feldspar and K-feldspar are commonly seen in the Xiashihezi and Shanxi Formations, with average values of approximately 5% and 10%, respectively. However, a sharp decrease in feldspar content occurs from the Taiyuan Formation to the Benxi Formation, with plagioclase feldspar barely perceptible in the Benxi Formation.

Quartzarenite is rarely observed in the study area, with the volume percentages of K-feldspar reaching almost 5% in the Taiyuan and Benxi Formations. This occurs for various reasons: (1) the study area is close to the source area of the Yimeng uplift, with a fraction of the plagioclase and K-feldspar still remaining because the transport distance was short (C. Lv et al., 2017); and (2) the sampled cores were recovered from the thick sandstones (potential reservoirs for tight gas), and the thin sandstones deposited during the rapid transgression period (with higher content of quartzarenite) were rarely sampled because they were not potential prolific gas reservoirs. The first reason is also supported by more than 20% (vol. %) of quartzites in

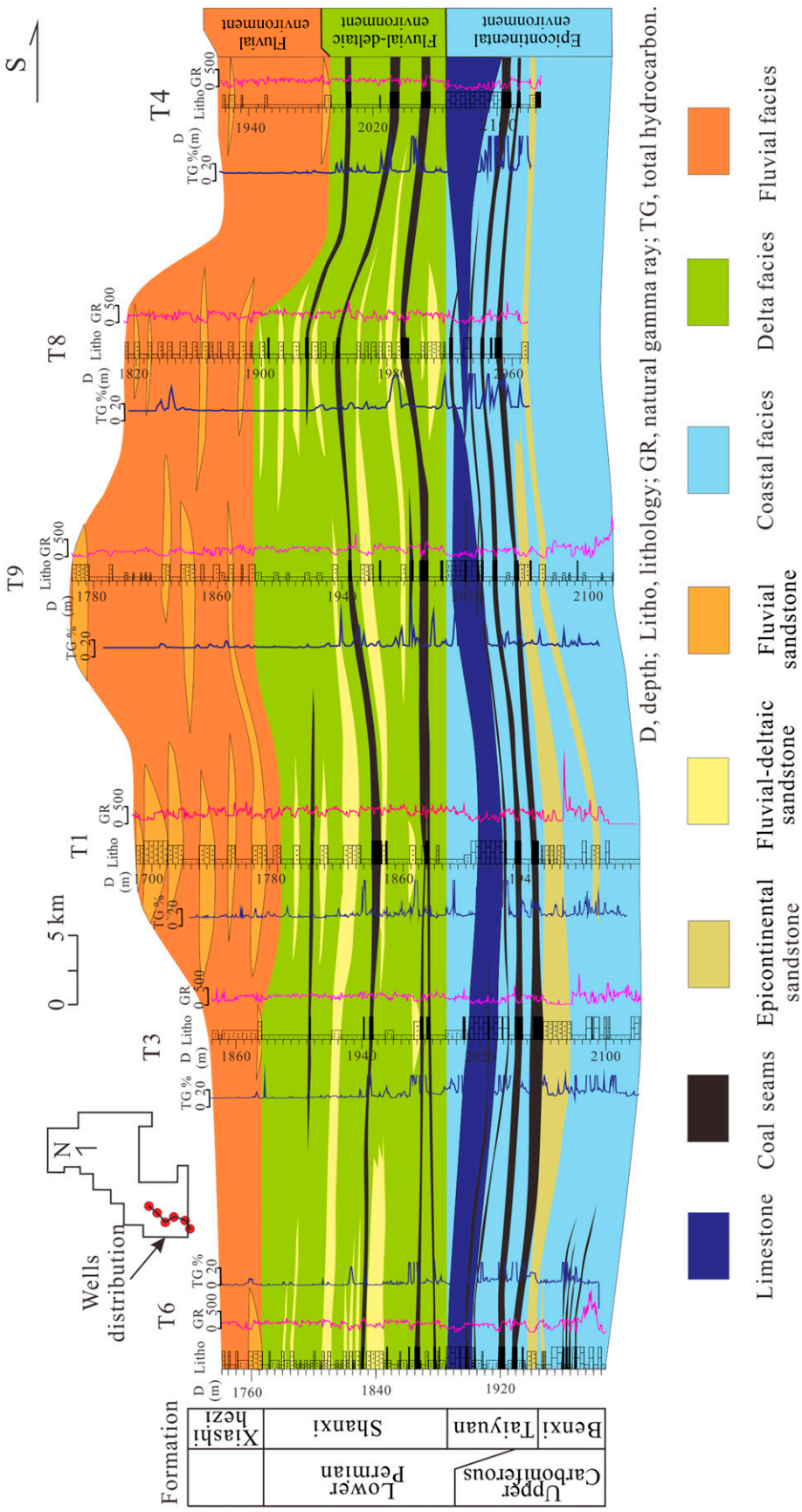

Figure 2. The partial cross-section representation of the upper Carboniferous to lower Permian (modified from Li et al., 2016). T = well names.

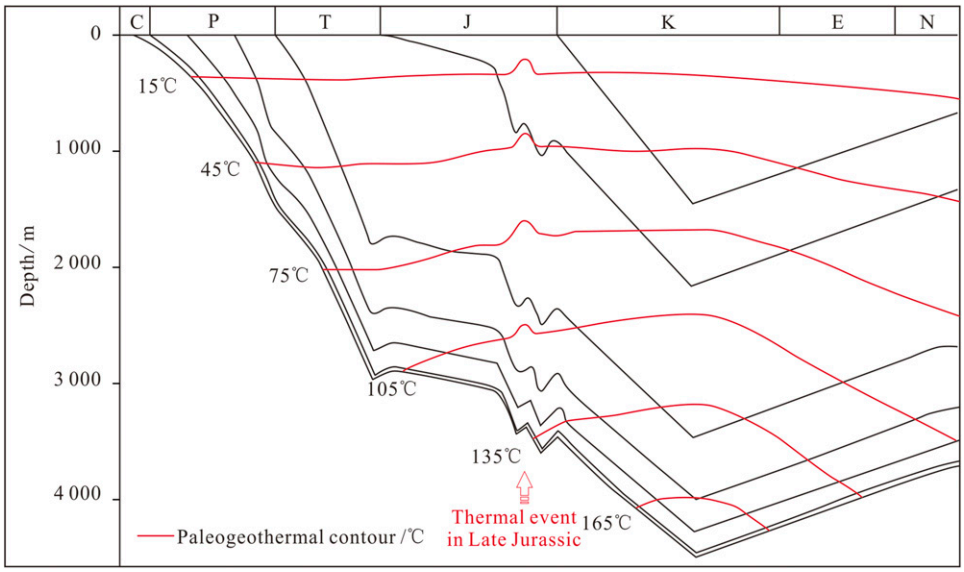

Figure 3. Burial and thermal histories of the Linxing area. C = Carboniferous; E = Eocene; J = Jurassic; K = Cretaceous; N = Neogene; P = Permian; T = Triassic.

all the formations and 10% (vol. %) of igneous rocks in the Xiashihezi and Shanxi Formations (Table 2).

Sandstone Properties

Porosity and Permeability

Porosity and permeability were measured by helium porosimetry and permeability experiments. These data indicate low values for all samples from the different formations. Approximately 85% of the samples show porosities below 10% (Figure 5A) and more than 90% of the samples have permeabilities below 1 md (Figure 5B). Similar results were reported by Li et al. (2016) in which helium-measured porosities ranged from 1.0% to 4.9% in the study area.

The porosity and permeability distributions of the different formations are shown in Figure 6. The Xiashihezi sandstones generally have higher porosity and permeability relative to the other units. As burial depth increases from 1200 to 2200 m (3937 to 7218 ft), the porosity of the sandstones decreases within each of the Shanxi, Taiyuan, and Benxi Formations (Figure 6A). The permeability shows no significant change with depth (Figure 6B). The sandstones of the Benxi Formation exhibit low porosities but relatively high permeabilities. Furthermore, it should be noted that the porosity of the sandstones in the Taiyuan Formation is generally higher than that of the Shanxi Formation.

The porosity and permeability of the sandstones are not only controlled by their burial depth but also by complex physical and chemical processes acting during their deposition and diagenesis. The separate impacts of compaction, cementation, and dissolution during diagenesis on porosity and permeability are discussed in the Diagenetic Mineralogy section.

Pore Types

The Xiashihezi Formation experienced weak compaction relative to that of the underlying strata, with a part of the primary intergranular porosity remaining (Figure 7A). Dissolution pores are common within the intergranular cements (Figure 7B, C). As burial depth increases, dissolution pores occur on feldspars and lithic fragments (Figure 7D, E) and also on detrital grain boundaries (Figure 7F). Both primary and secondary pores are well developed in the sandstones of the Xiashihezi Formation, rendering a relatively higher porosity than that of the other strata.

The primary pores are difficult to distinguish in the sandstones of the Shanxi Formation, with quartz overgrowths widely distributed (Figure 7G). Siderite and other minerals fill parts of the pores (Figure 7H). Feldspar dissolution is well developed, with some

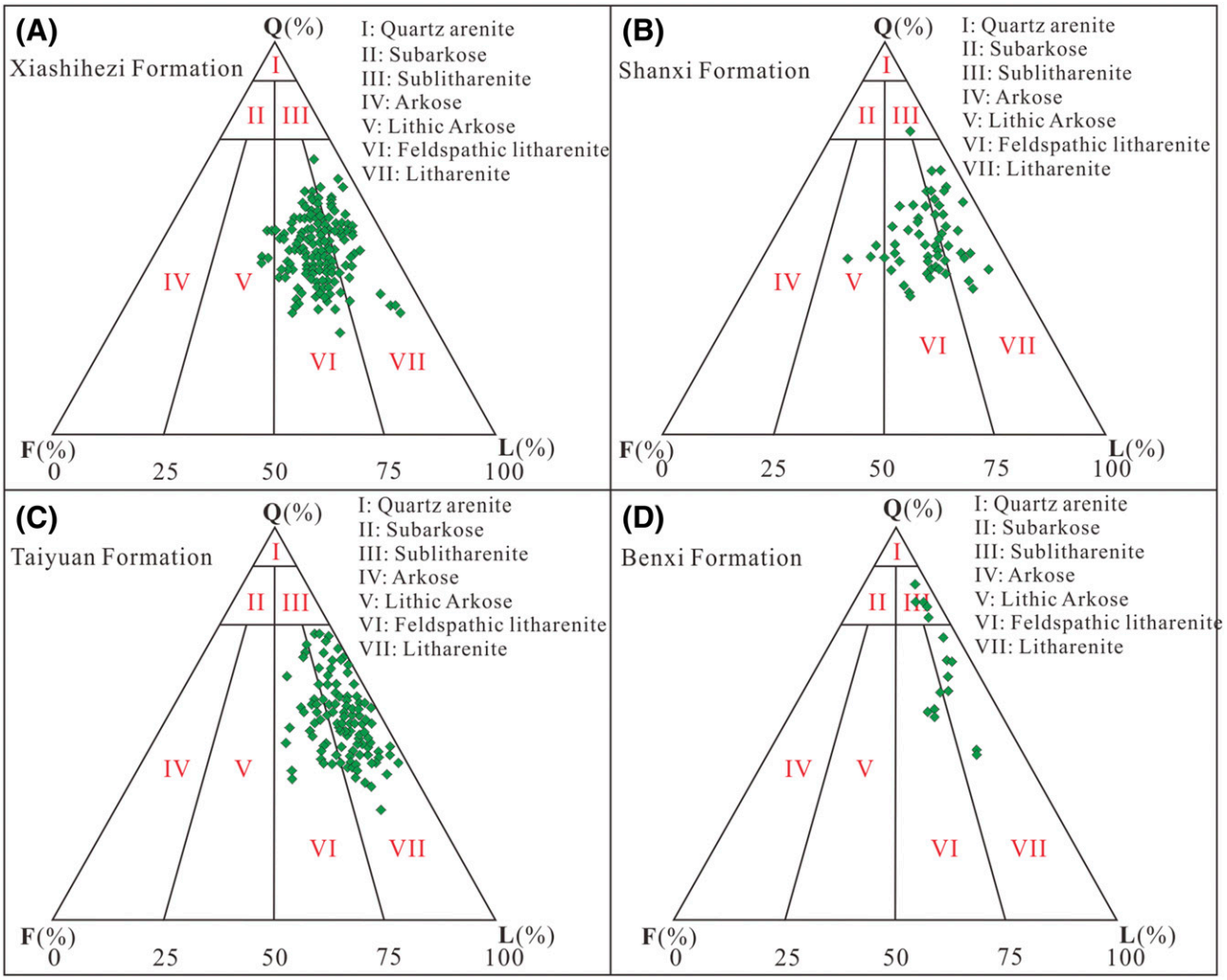

Figure 4. Rock composition of sandstones from different formations in the Linxing area. (A) Xiashihezi Formation; (B) Shanxi Formation; (C) Taiyuan Formation; (D) Benxi Formation. The ternary plot refers to the sandstone classification standard of Folk et al. (1970). The green diamonds represent rock composition plots of different samples. F = feldspar; L = lithic fragments; Q = quartz and chert.

feldspars transformed into kaolinite and other clay minerals (Figure 7I). The results show that the Shanxi Formation has undergone strong compaction, with dissolution effects also having important significance in the development of porosity.

Quartz overgrowths are also extensively developed in sandstones of the Taiyuan Formation, partially represented by mosaic cementation. However, the dissolution effect is strong, with lithic and quartz grains being dissolved (Figure 7J, K). This also explains the higher apparent porosity of sandstones in the Taiyuan Formation relative to those from the Shanxi Formation (Figure 6). Furthermore, fractures are relatively well developed in the Taiyuan Formation, which may also contribute to the higher porosity and permeability.

Thin sections from the Benxi Formation show no large differences in pore compositions (not shown).

Diagenetic Mineralogy

Apparent from the various pore morphologies, the sandstones have undergone various diagenesis processes. Compaction, dissolution, and cementation of silicates and carbonates and the transformation of the authigenic clay minerals are apparent.

Compaction

Compaction occurs soon after deposition, and the continuously deposited material results in water

Table 1. Rock Compositions of Sandstones from Different Formations with Data Plotted in Figure 4

Sample Nos.	Formation	Percentage of Different Rock Types, %				
		Quartzarenite	Sublitharenite	Lithic Arkose	Feldspathic Litharenite	Litharenite
159	Xiashihezi	–	–	2	75	23
59	Shanxi	–	2	6	57	35
121	Taiyuan	5	–	–	22	73
16	Benxi	5	35	–	24	36

Abbreviations: – = not applicable; Nos. = numbers.

discharge of the lower strata, which manifest as the sediment volume and porosity both reduce (e.g., Lundegard, 1992; Ramm, 1992; Fisher et al., 1999). Compaction generally shows a strong effect at depths less than 2500 m (<8202 ft), with the intergranular pore volume declining abruptly from approximately 40% at the surface to approximately 28% at 1500 m (4921 ft) (Paxton et al., 2002). Thus, the decrease in porosity from depths of 1200 to 1500 m (3937 to 4921 ft) in Figure 6 likely results from compaction, which is apparent in thin sections (Figure 8). Significantly, grain intergrowths are apparent on the detrital grains (Figure 8A), with contact edges deformed into concave-convex interfaces. The small grains and detrital material are tightly packed, with no spare pores (Figure 8B). The soft sedimentary rocks have been deformed and reshaped as the mica in Figure 8C and the argillaceous and ferrous cements show a directional distribution perpendicular to the compaction stress (Figure 8D).

Quartz Cement

Quartz cement commonly occurs as pore-filling cement with syntaxial overgrowths around detrital quartz grains. Secondary enlargement around quartz is observed under polarized light microscopy (Figure 9A, B), with the contours of the original clasts identified by a remnant clay film left at the edge of the grains. The optical orientation of the secondary enlarged side agrees with the original quartz grains. Authigenic quartz occludes intergranular and dissolution pores, decreasing the porosity and bridging narrow pore throats (Figure 9C, D). Quartz overgrowth partly occurs together with authigenic clay minerals such as the illite in Figure 9C and kaolinite in Figure 9D. The boundaries of the detrital quartz grains and the cements are typically traced by fluid inclusions, irregular corrosion, and clay coatings (Figure 9A, B).

Clay Minerals Cement

Clay minerals, including kaolinite, illite, chlorite, and minor amounts of Fe-rich clays, generally coat the surfaces of particles or are seen as authigenic shapes infilling the pores. The authigenic clay minerals are mainly kaolinite, chlorite, illite, and illite–smectite (I/S). The euhedral shape of the kaolinite shows booklet and helminthoid filling in the intergranular and dissolved pores that are enveloped by, and thus predate, quartz overgrowths (Figure 10A, B). As the burial depth increases, the surface of the kaolinite

Table 2. Statistical Table of the Relative Contents of Clastic Components of the Upper Paleozoic Sandstone in the Linxing Area

Sample Nos.	Formation	Detrital Components, %										
		Q	C	Pf	K-f	Rs	Ri	Rm	Qd	Mica	Hm	Sum.
165	Xiashihezi	45.5	0.7	5.6	10.7	0.4	10.2	2.1	23	1.1	0	100
65	Shanxi	47.5	1.2	4.6	10.1	0.2	11.2	1.3	22.7	1.2	0	100
135	Taiyuan	50.8	1.2	3.5	5.2	0.6	7.4	1.1	29.7	0.3	0	100
16	Benxi	65.1	2.1	0.7	6.2	0	2.2	1.4	22.1	0.3	0	100

Abbreviations: C = chert; Hm = heavy mineral; K-f = K-feldspar; Nos. = numbers; Pf = plagioclase feldspar; Q = quartz; Qd = quartzite debris; Ri = igneous rock; Rm = metamorphic rock; Rs = sedimentary rock; Sum. = summary.

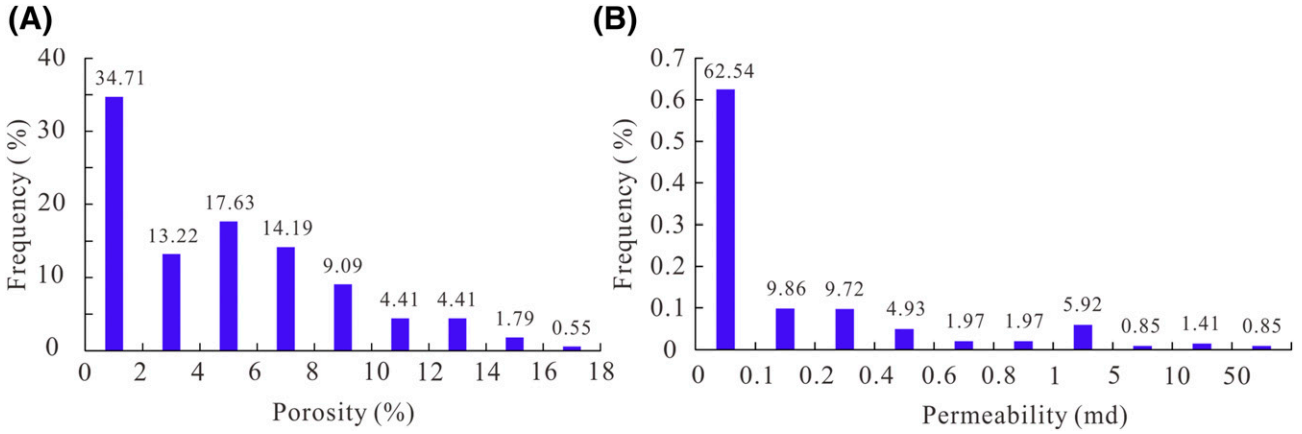

Figure 5. The helium-derived (A) porosity and (B) permeability distributions of different ranges.

is covered with hairlike illite, indicating that the kaolinite is transforming into illite (Figure 10D, E). Chlorite has a good idiomorphic degree (in the shape of a rose petal) and is attached to the surfaces of the clastic particles. Microcrystalline Fe-rich chlorite rims are found around the detrital feldspar grains (Figure 10J). The surface of the authigenic quartz also grows with chlorite, showing that the chlorite postdates the overgrowth of quartz (Figure 10I).

In the shallow strata, the illite is generally flaky and attached to grain surfaces (Figure 10E), but as depth increases, the illite occurs as fibrous pore-lining crystals, together with Fe-calcite (Figure 10F) and authigenic quartz (Figure 10I). The I/S layering is a product of smectite transforming into illite and occurs as honeycomb filling-in of the pores (Figure 10C). As depth increases, the I/S layers gradually transform into illite, and the smectite in the I/S mixed layer decreases gradually until completely exhausted.

The total volume content of clay minerals is high in the study area and comprises sedimentary clay deposits and authigenic clay minerals generated during diagenesis. The total clay mineral content increases with increasing burial depth; however, the content of different clay minerals (kaolinite, illite, chlorite, and I/S) shows different trends (Figure 11). With increasing burial depth, the relative content of kaolinite shows a trend that increases, decreases, then increase (Figure 11A), whereas the volume contents of chlorite and I/S mixed layers decrease consistently with increasing depth (Figure 11B). The top of the Xiashihezi Formation exhibits the highest content of illite and decreases gradually as burial depth increases (Figure 11C). The I/S mixed layer decreases from 75% to 15%, indicating a gradual transition from a disordered layering to an ordered mixed layer. This phenomenon indicates that the tight sandstones of the Taiyuan Formation entered a mesodiagenetic stage.

Carbonate Cement

Carbonate cements are volumetrically predominant, including calcite, Fe-calcite, and ankerite, as well as a small amount of siderite. Calcite and Fe-calcite are generally present as rhomboids or mosaic shapes infilling the pores (Figure 9E, G). The Fe-calcite can be seen deposited within the dissolved feldspar and on the edges of quartz overgrowths (Figure 9E, L). The calcite, which is microcrystalline to sparry, grows over, envelops, and therefore postdates the quartz overgrowths in the large intergranular pores (Figure 9H). Ankerite occurs as sparry and coarse-crystalline cement and partly or completely infill the large intergranular pores (Figure 9F). Siderite intraclasts are massive and developed with crystallites (Figure 9K). Other siderite intraclasts are rounded and overgrown by euhedral siderite cements and partly or completely fill the intergranular pores (Figure 9I).

Other Cements

Pyrite is a minor cement that was observed in thin sections and in cores. The formation of pyrite requires certain amounts of sulfur, which is most readily supplied by a flux of H_2S derived from the breakdown of sulfur-bearing organic material during the early phases of maturation of organic matter in a reducing environment (Al-Ramadan et al., 2005; Karim et al., 2010). Pyrite is not only seen in the

Taiyuan and Benxi Formations, which were deposited in an epicontinental environment, but also in the Shanxi Formation, which represents a fluvial-deltaic environment. Pyrite framboids fill intergranular pores or occur over the carbonate cements (Figure 9J), which probably formed during early and late stages, as apparent in other studies (El-ghali et al., 2006; Xi et al., 2015a). Ferruginous cements are apparent as microscopic black mineral grains, such as ferruginous clay strips (Figure 9I) and mud crystal siderite (Figure 9K).

Dissolution

Apart from the sandstones in the Xiashihezi Formation, most of the sandstones present no primary intergranular pores; the pores mainly comprise secondary pores generated during the dissolution process (Table 4). The dissolution is confined mainly to feldspars (Figure 12A, B) and lithic fragments but also to cements (e.g., calcite dissolution in Figure 12C). Furthermore, as the burial depths increase, the quartz also shows dissolution (Figure 12D), with illite occurring on quartz grains.

Figure 12B shows an ongoing process of feldspar dissolution, whereas the feldspar in Figure 12A has been generally dissolved and is transforming into kaolinite. The surface porosity (by volume) evaluated from microscopy ranges between 3% and 4%. The Shanxi Formation presents the lowest value (3.07%), and the Taiyuan Formation presents the highest (4.23%) (Table 4). The dissolution of feldspar is accompanied by the formation of clay minerals and is commonly accompanied by microcrystalline kaolinite and quartz overgrowths. The illite and authigenic quartz are generally generated in deeper strata, locally with visible chlorite filling of dissolution pores.

DISCUSSION

Diagenetic Controls on Reservoir Quality

Impacts of Clay Minerals on Pores

Positive Impacts—Different kinds of minerals show different effects on pore evolution throughout the

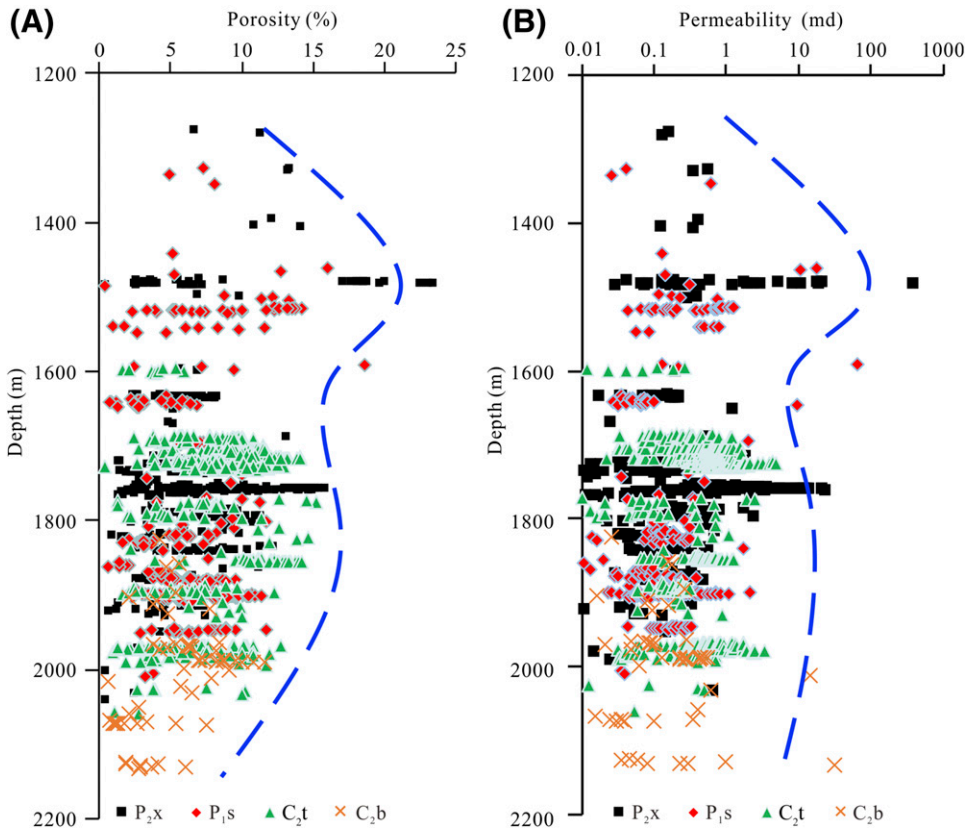

Figure 6. (A) Porosity and (B) permeability variations with depth for samples collected from different formations in the study area. The dashed blue line represents the brief variation trend. C_2b = Benxi Formation; C_2t = Taiyuan Formation; P_1s = Shanxi Formation; P_2x = Xiashihezi Formation.

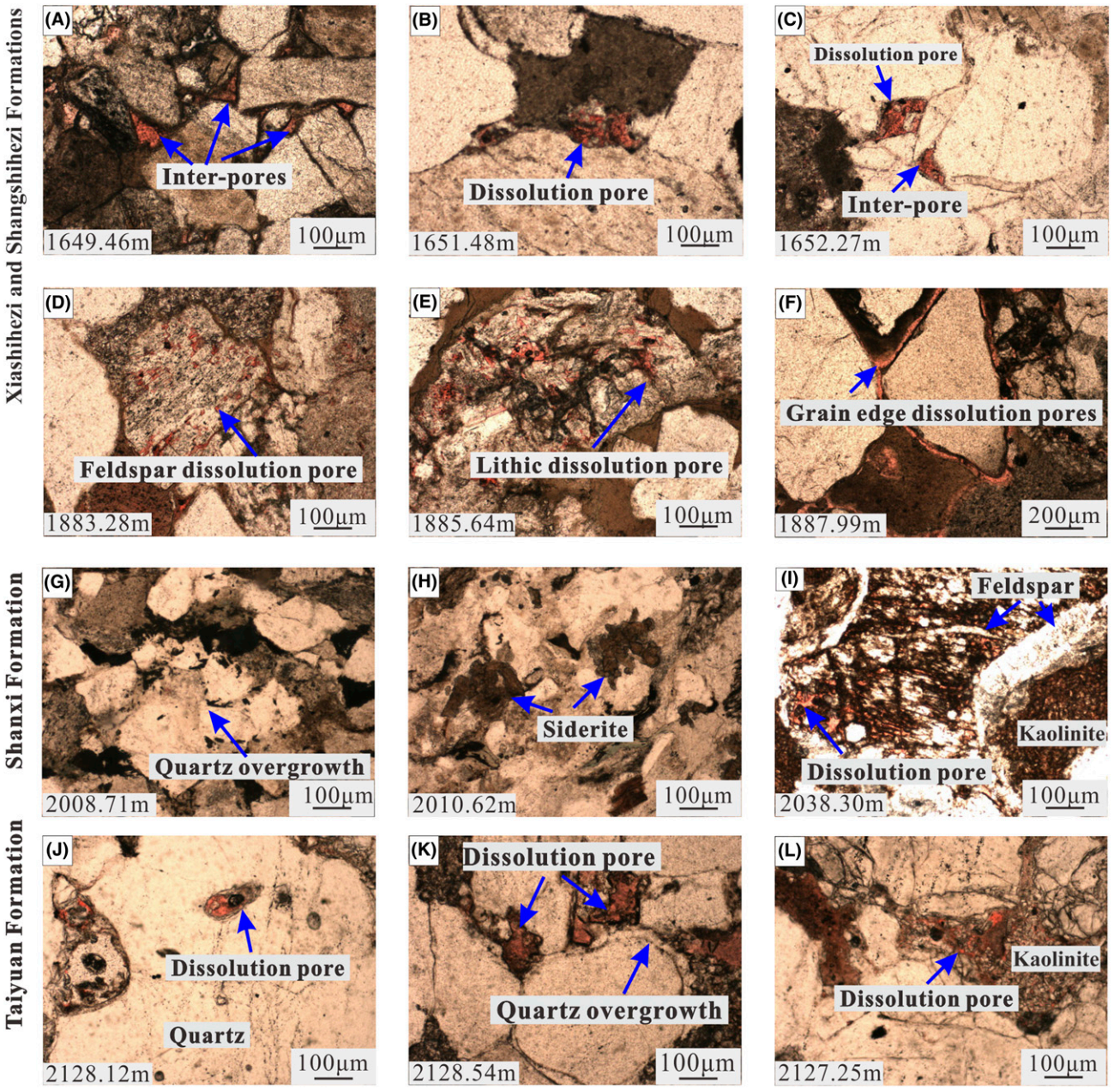

Figure 7. Pore types of the tight sandstone reservoirs. All the sections were selected from well T2, which is located in the southwestern part of the study area, and the depths are marked. (A) interpores; (B) dissolution pores; (C) interpores and dissolution pores; (D) feldspar dissolution pore; (E) lithic dissolution pores; (F) grain edge dissolution pore; (G) quartz overgrowth; (H) siderite; (I–L) dissolution pores.

entire diagenetic process (Ece et al., 2013; Zhu et al., 2016). Several studies have reported that previously formed chlorite rims developed on quartz grains preserve porosity in sandstones, as reported from the overpressured reservoirs of the Mississauga Formation of the Venture and Thebaud fields (Gould, 2007). Chlorite formed during the eodiagenesis stage is generally a film wrapped around the edges of grains. This diagenesis both reduces the intergranular porosity as a cement but enhances the stability between particles, which reduces the damage caused by compaction on intergranular pores and acts to stem further reduction in porosity. This partly explains the existence of residual intergranular pores in the tight reservoirs of the Xiashihezi Formation.

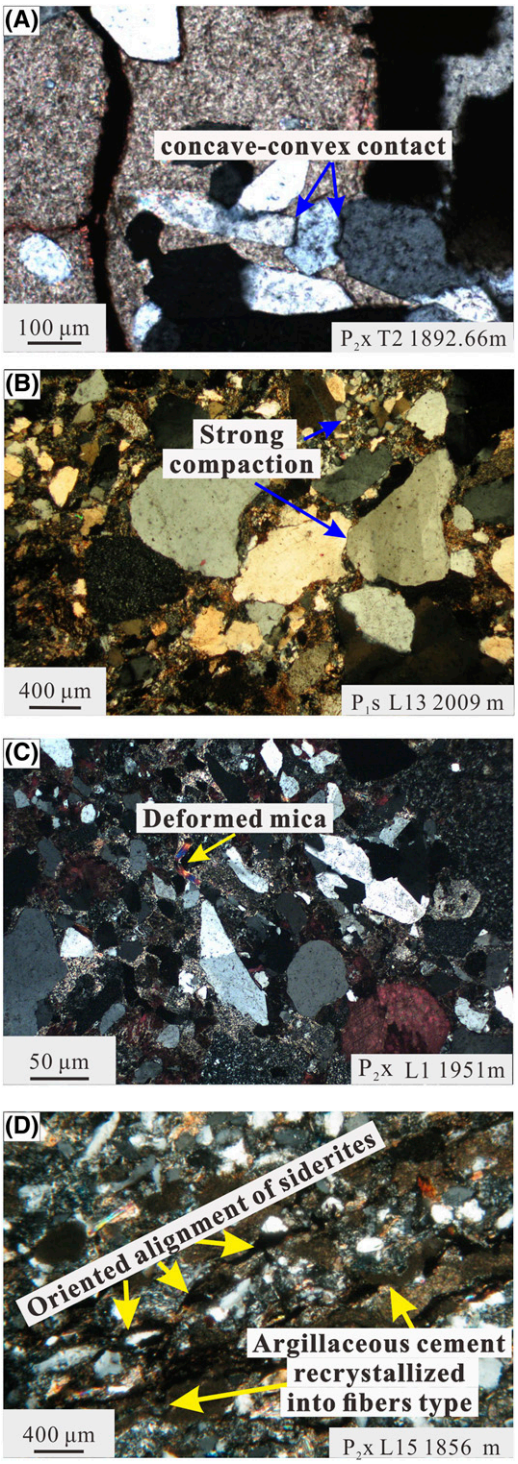

Figure 8. Characteristics of compaction in the study area. (A) Grains contacted in a concave–convex structure; (B) strong compaction of quartz grains, small grains, and lithic fragments closely compacted; (C) volcanic rocks, grains compacted and deformed, metasomatic Fe-calcite in lithic fragments, and pore infillings; (D) silty structure, quartz, feldspar, and argillaceous siderites. L = well name; P_1s = Shanxi Formation; P_2x = Xiashihezi Formation; T = well name.

We found that silica cement has a similar effect. In the Taiyuan Formation, quartz secondary enlargements and authigenic quartz particles are well developed, and the framework particles are mosaicked. The silica cementation enhances the strength of the skeleton of sandstone particles, which leads to the preservation of intergranular pores in the tight reservoirs of the Taiyuan Formation. This partly explains why the porosity of the Taiyuan Formation is higher than that of the Shanxi Formation. Furthermore, siderite cement inhibits the formation of quartz overgrowths and thus contributes to the preservation of porosity (as noted by Rossi et al., 2001 and Karim et al., 2010).

Negative Impacts—Although the chlorite and quartz show some positive effects in preserving intergranular porosity, most of the clay minerals show a negative effect on porosity and permeability. Overall, the porosity and permeability of tight sandstones decrease with the increase of the clay mineral content. Low-porosity sandstones are generally cemented by quartz overgrowths and by kaolinite and carbonate cements (including siderite), which significantly decrease porosity (Jansa and Urrea, 1990).

The kaolinite cements are generally present as hexagonal crystals, and the aggregates are generally vermicular and accordionlike. They are formed in acidic diagenetic environments and reduce reservoir porosity (Zhu et al., 2008). Chlorite cements, mainly generated in the late stages of diagenesis, are generally leaflike and filamentous and generally grow along grain surfaces; these greatly reduce the permeability of the reservoir (Cao et al., 2018). Pyrite cementation mainly develops in strong reducing environments, which are causally related to the distribution of organic matter or hydrocarbons (Worden et al., 2003). The pyrite cements in the study area are generally formed in the late stages of basin evolution and have regular octahedral shapes (under SEM).

Impact of Dissolution on Pores—Dissolution is an important diagenesis process that typically increases both porosity and permeability and, as such, improves reservoir quality (de Melo et al., 2015; Ma et al., 2017). During the maturation of organic matter (coal and dark shales) in the Taiyuan Formation, a large amount of organic acid is generated during the

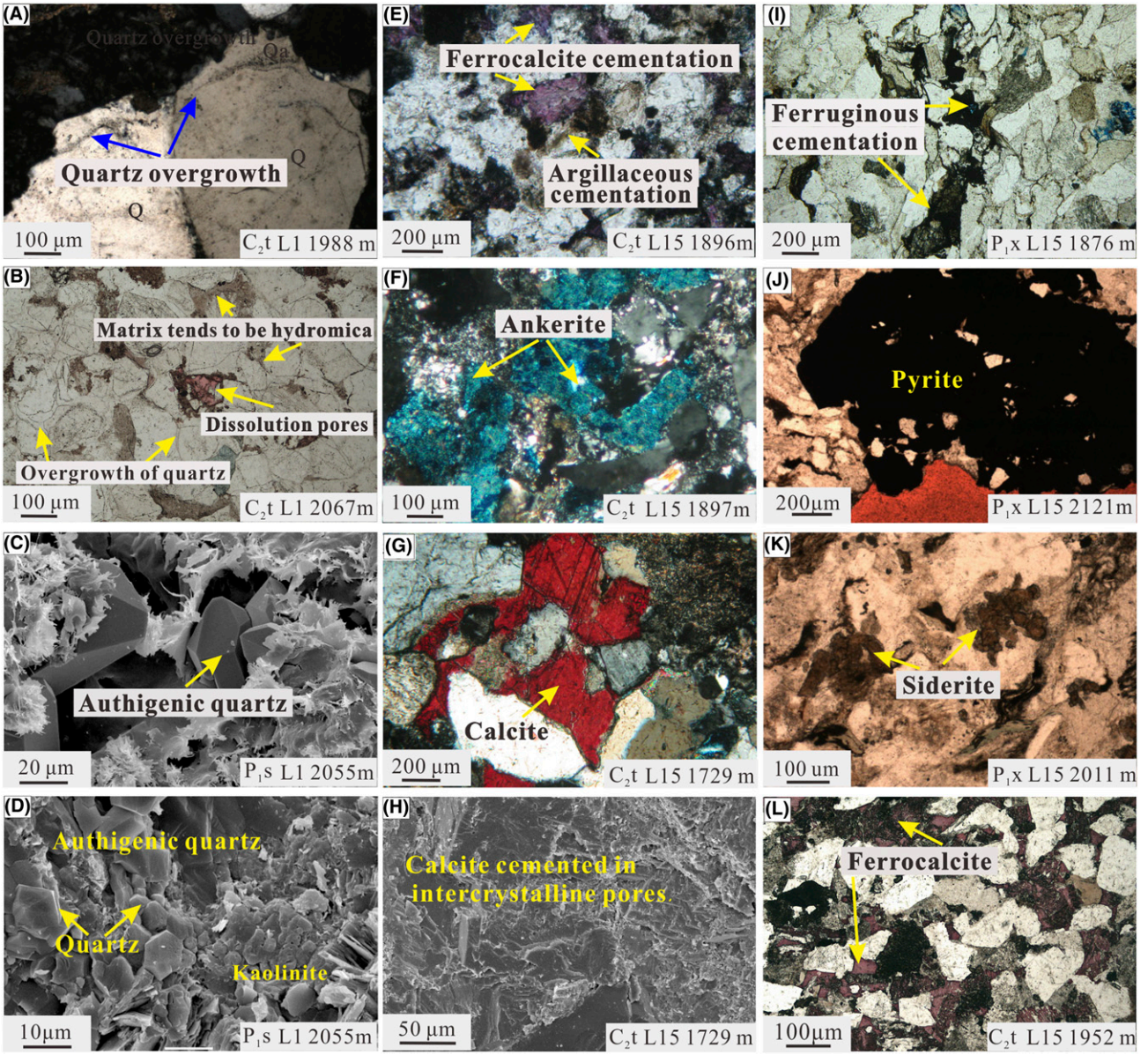

Figure 9. Silicate, ferruginous, and carbonate cements in the tight sandstone. (A) Quartz (Q) overgrowth (Qa) with observed original boundary; (B) dissolution pores and quartz secondary enlargement; (C) pore-filling authigenic quartz that is euhedral crystallized; (D) authigenic quartz occurred with booklike kaolinite; (E) Fe-calcite filling intergranular pores; (F) sparry and coarse-crystalline ankerite filling in intergranular pores; (G) microcrystalline calcite and sparry calcite; (H) calcite filling intercrystalline pores; (I) siderite filling in intergranular pores; (J) cluster pyrite shown as a black mineral grain; (K) massive siderite clasts; (L) Fe-calcite filling in dissolution pores. C_2t = Taiyuan Formation; L = well name; P_1s = Shanxi Formation; P_2x = Xiashihezi Formation.

coalification and thermal evolution process, together with CO_2 (Li et al., 2017b). These acids react with the limestones in the Taiyuan Formation and result in dissolution of feldspars, lithic fragments, and cements, creating secondary pores (Table 4).

Dissolution by organic acids also exerts a largely negative effect on reservoir porosity, permeability, and therefore quality. The early-deposited calcite and chlorite cements can enhance the skeletal strength and stiffness of sandstones (Wang et al., 2017), but their dissolution can obviate this positive effect in resisting compaction, resulting in increased damage to residual intergranular pores. Furthermore, after dissolution, the quartz particles remain exposed and are subject to a wide range of possible developments for secondary enlargement (Lai et al., 2017).

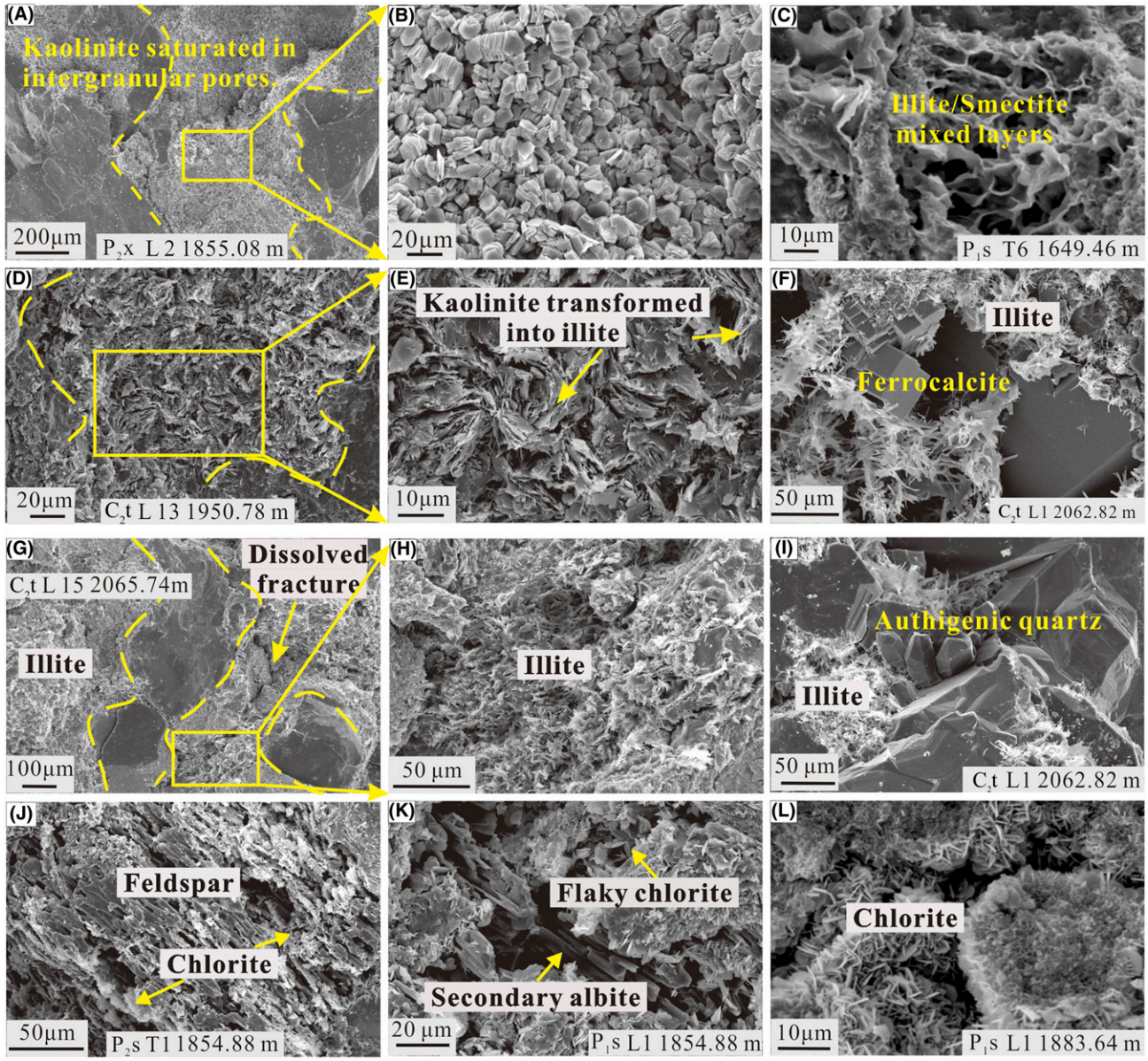

Figure 10. Clay minerals in the tight sandstone imaged by scanning electronic microscopy. (A, B) Euhedral kaolinite in intergranular and dissolved pores; (C) honeycomb illite–smectite mixed layers; (D, E) kaolinite connected to hairlike illite; (F) fibrous illite occurring as crystals with Fe-calcite; (G, H) illite filling in dissolution fracture; (I) fibrous illite formed after authigenic quartz; (J) microcrystalline chlorite rims found around the feldspar grains; (K) flaky chlorite occurring together with secondary albite; (L) chlorite in the shape of a rose petal. C_2t = Taiyuan Formation; L = well name; P_1s = Shanxi Formation; P_2s = Shangshihezi Formation; P_2x = Xiashihezi Formation; T = well name.

The Transformation of Diagenetic Clay Minerals and Its Correlation with Porosity—The porosity of the tight sandstone reservoir is strongly influenced by the effects of compaction, cementation, and dissolution (Rahman and Worden, 2016). The original porosity is reduced by compaction and cementation, and the dissolution of the grain skeleton or framework increases the porosity of the reservoir to a certain extent. As the diagenetic process proceeds, the pore combinations comprising the reservoir progress from single primary intergranular pores to combinations of primary pores, then secondary pores, then intercrystalline pores in clay minerals. The final disposition of pore types comprises secondary pores and intercrystalline pores in clay minerals as present in the study area.

Different clay mineral transformations have proceeded in the different formations with different

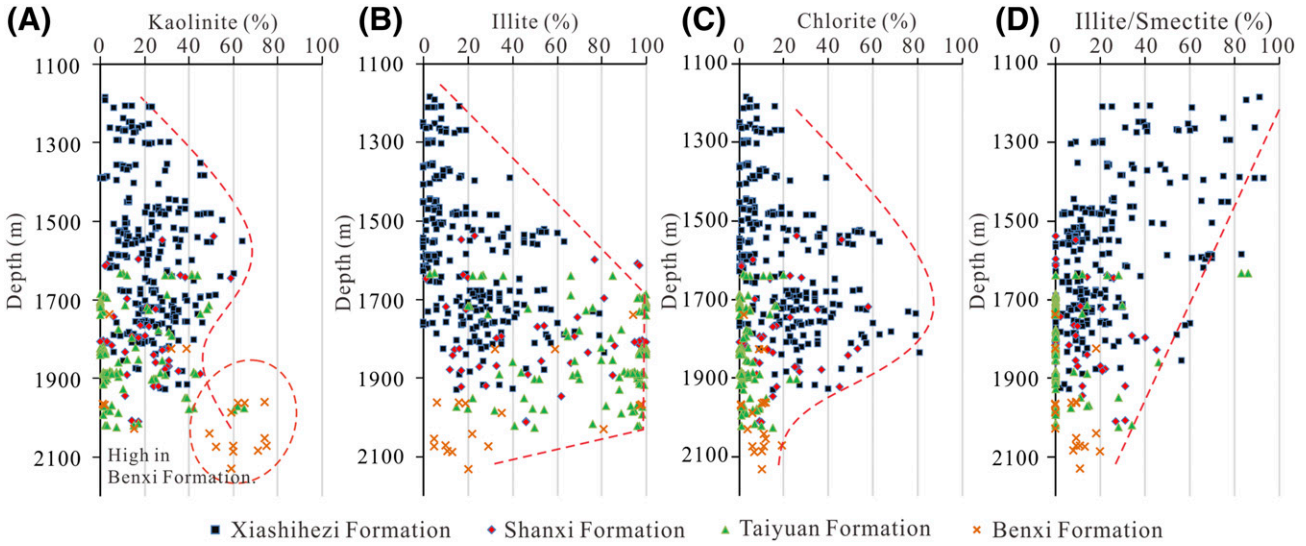

Figure 11. Relative contents of different clay minerals with increasing depth. (A) Kaolinite; (B) illite; (C) chlorite; (D) illite/smectite mixed layers. Dashed red lines represent brief variation trends.

impacts on the terminal porosity and permeability (Wang et al., 2017). In the Shanxi and Taiyuan Formations, for example, the feldspar surfaces are easily dissolved, and these formations evolve with relatively well-developed dissolved pores (Figure 13A). As time progresses, part of the feldspar and grain cements are completely transformed into kaolinite, which obstruct the pores and pore throats (Figure 13B). The kaolinites of the Shanxi Formation (Figure 13C) exhibit euhedral crystalline, booklet, and six plate forms with well-developed intergranular pores. In most of the samples, however, kaolinite (tending to illite) fills in the intergranular pores with euhedral quartz overgrowths, and the porosity is substantially decreased (Figure 13D).

The sandstones in the Taiyuan Formation show a relatively higher degree of diagenesis, with platy kaolinite infilling the intergranular pores and with well-developed intercrystalline pores (Figure 14A). Part of the kaolinite is dissolved, with pores being more developed (Figure 14B), which, to some extent, explains the relatively high porosity of the sandstones of the Taiyuan Formation (Figure 6). The kaolinite is transforming into illite, with hairlike illite filling the pores and with quartz overgrowths (Figure 14C). Part of the illite retains a honeycomb structure, indicating that it has been transformed from smectite (Figure 14D).

Timing of Diagenetic Processes

It is difficult to determine the exact timing of the various diagenetic processes, but the sequence of diagenetic events can be established from the lithofacies structure and stratigraphic burial history (Mansurbeg et al., 2008). Indices associated with the classification of diagenesis process associated with clastic rocks include (1) the structural characteristics and pore types of the sandstones and the contact relationships between the particles; (2) the formation sequences and distribution of authigenic minerals; (3) the combination of clay minerals; (4) the paleo temperature (recovered from the homogenization temperatures of fluid inclusions observed mainly in the fractures of quartz); (5) the degree of conversion of clay minerals in the I/S mixed layers; and (6) the maturity of organic matter, together with other factors (Zhu et al., 2008; Schmitt et al., 2015).

Eodiagenesis

The tight sandstone reservoir in the study area has experienced mesodiagenesis, but the type and extent of eodiagenesis directly influenced the development of later diagenesis as well as the ensuing reservoir properties (El-ghali et al., 2006). The eodiagenesis mainly involved the mechanical compaction of detrital particles, cementation of siderite and clay minerals, and dissolution of the unstable detrital particles (Figure 15).

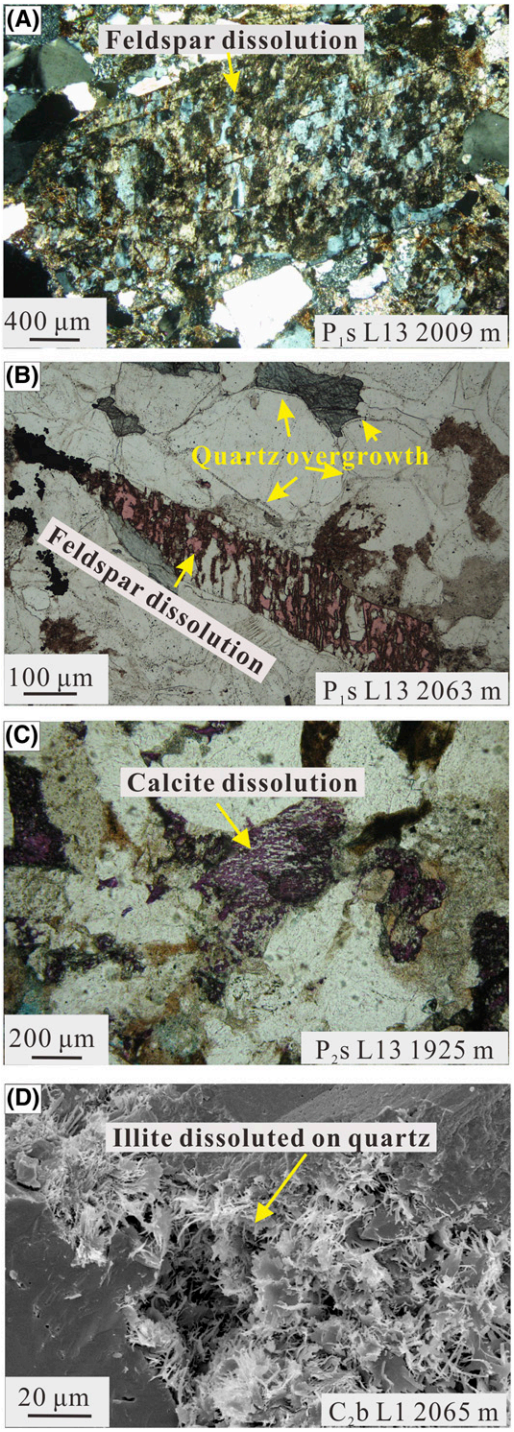

Figure 12. Dissolution pores in the tight sandstones. (A) Feldspar dissolution, partly replaced by kaolinite; (B) feldspar dissolution pores, observed ongoing dissolution process, and quartz overgrowth caused by the pressure solution (pointed at by the arrows); (C) calcite dissolution pores and poorly crystallized chlorite; (D) quartz showing a kind of dissolution and illite on quartz grains. C_2b = Benxi Formation; L = well name; P_1s = Shanxi Formation; P_2s = Shangshihezi Formation.

As the sedimentation and burial depth increased, increased overburden pressure gradually compacted the assemblage and rearranged the particles, with the excess pore water expelled (Bjørlykke, 2014). Thin sections enable the observation of directional alignments of the framework of particles and deformation of mica and nonrigid particles (Mansurbeg et al., 2008). The contacts between the particles comprising the structural framework also gradually change from point contacts into line contacts, resulting in reductions of intergranular porosity (Hakimi et al., 2012, 2013). In the Xiashihezi and Shanxi Formations, the contacts between particles in the tight reservoir are mostly from planar to concave–convex, with commonly seen directional alignments of feldspars and extrusion deformations of nonrigid lithic fragments such as mica (Figure 8). All of the above observations indicate that mechanical compaction has significantly damaged or reduced the porosity of the tight reservoir (Figure 15).

Mesodiagenesis

The mesogenetic minerals are controlled by the trapping of basinal fluid and influenced by the presence of hydrocarbons, together with temperature, pressure, and the characteristics of lithofacies, including any basinal inversions (Karim et al., 2010).

Pyrite and siderite are both present in the mesogenic stage (Figure 16; Karim et al., 2010), with chlorite widely presented as chlorite rims and fibrous pore-filling chlorite. Studies have shown that the dissolution of siderite is a source of Fe for chlorite (Iijima and Matsumato, 1982), and the conversion of berthierine to chlorite occurs at temperatures above 70°C–100°C (Worden and Morad, 2009). Furthermore, chlorite rims evolve into fibrous pore-filling illite (Figure 10L), which are mesogenetic minerals. The pore-filling chlorite and illite are precipitated later than the quartz overgrowths but postdate the carbonate cements. The chlorite content decreases linearly as depth increases in this study area (Figure 11C). The chloritization of kaolinite may occur at 165°C–250°C (Boles and Franks, 1979) or 100°C (Curtis et al., 1985), as recognized from different basins. But the variations in chlorite and kaolinite contents show no correlation here (Figure 11A, C). The Benxi Formation shows quite limited chlorite content, which may result from the

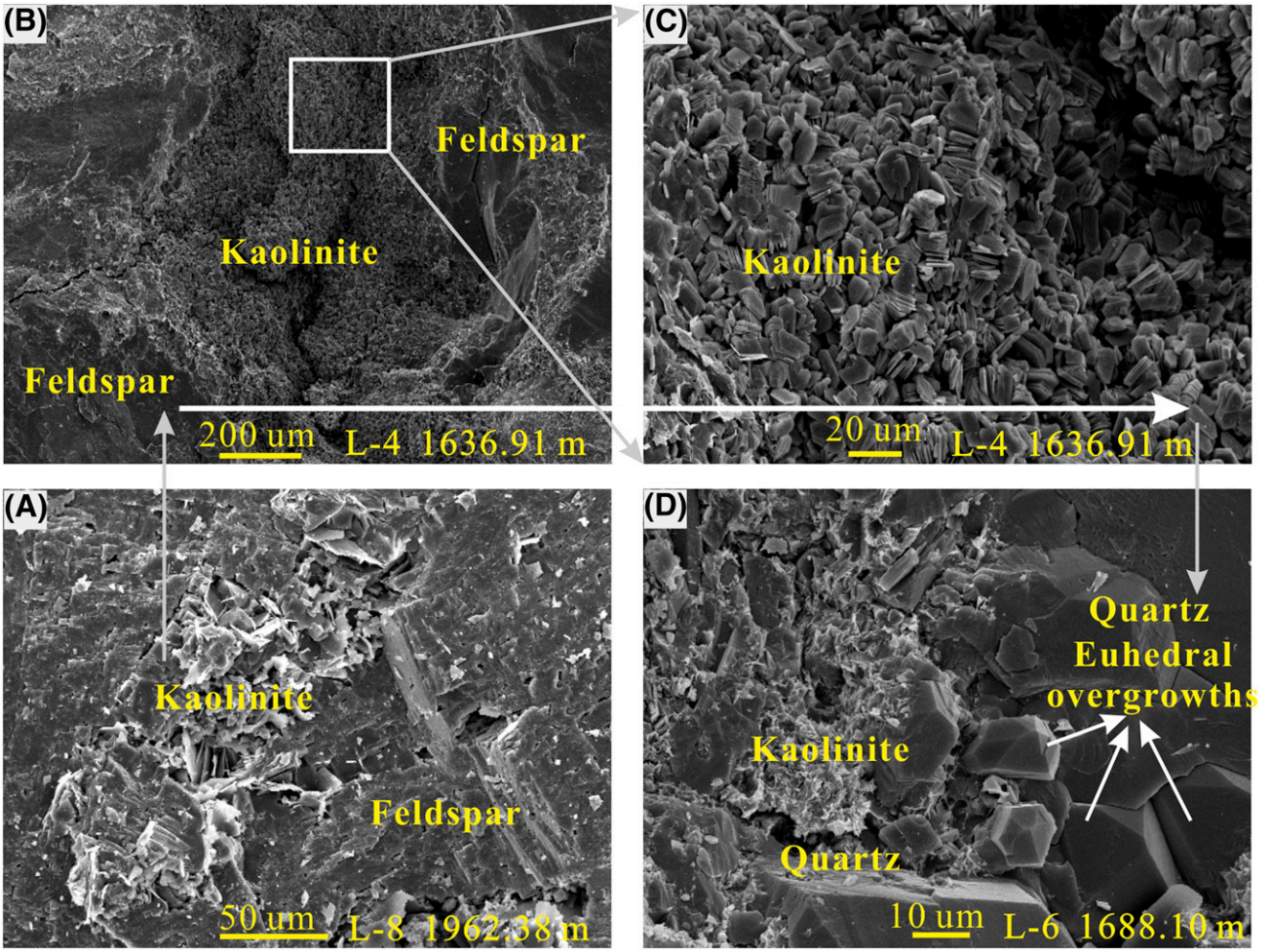

Figure 13. Influence of clay minerals on pore structure development in the Shanxi Formation. (A) Surface of feldspar being dissolved; (B) part of the feldspar and cements have been completely transformed into kaolinite; (C) the kaolinite shows quite good euhedral crystalline, booklet, and hexagon shapes, with well-developed intergranular pores; (D) kaolinite (transforming to illite) fills in the intergranular pores, with euhedral quartz overgrowths. L = well name.

acidic environment resulting from the coalification process. Furthermore, siderite is readily dissolved by the CO_2 generated during the early coalification process (Li et al., 2017b) and increases the concentration of Fe^{2+} in the basin fluids.

A total of 36 fluid inclusion samples from the sandstones and limestones were tested to constrain temperature variations during diagenesis, including the time of hydrocarbon generation and the necessary temperatures of mineral precipitation (Hendry et al., 2000; Rahman and Worden, 2016). The fluid inclusion data indicate that there are two major phases of hydrocarbon generation, with the corresponding temperatures of peak hydrocarbon generation at approximately 125°C–135°C and 160°C, respectively (Figure 16). The first stage of hydrocarbon generation was caused by magmatism concurrent with the Yanshanian movement, and the second stage of hydrocarbon generation was mainly caused by the maximum burial depth (Gao et al., 2018).

The mesogenetic carbonate cements include ankerite, Fe-calcite, and calcite. The carbonate cements are correlated with the CO_2 generated during the decarboxylation of organic matter in coal or the dark shales in the coal-bearing strata and corresponding abundant Ca^{2+}, Mg^{2+}, and Fe^{2+} ions in the formation water because the strata are less permeable for large ions than for CH_4 or CO_2 (Karim et al., 2010). Methane generated in the early stages of hydrocarbon maturation produce dissolved Fe from iron oxides and hydroxides until the iron oxides are exhausted. Ankerite and illite are generated at

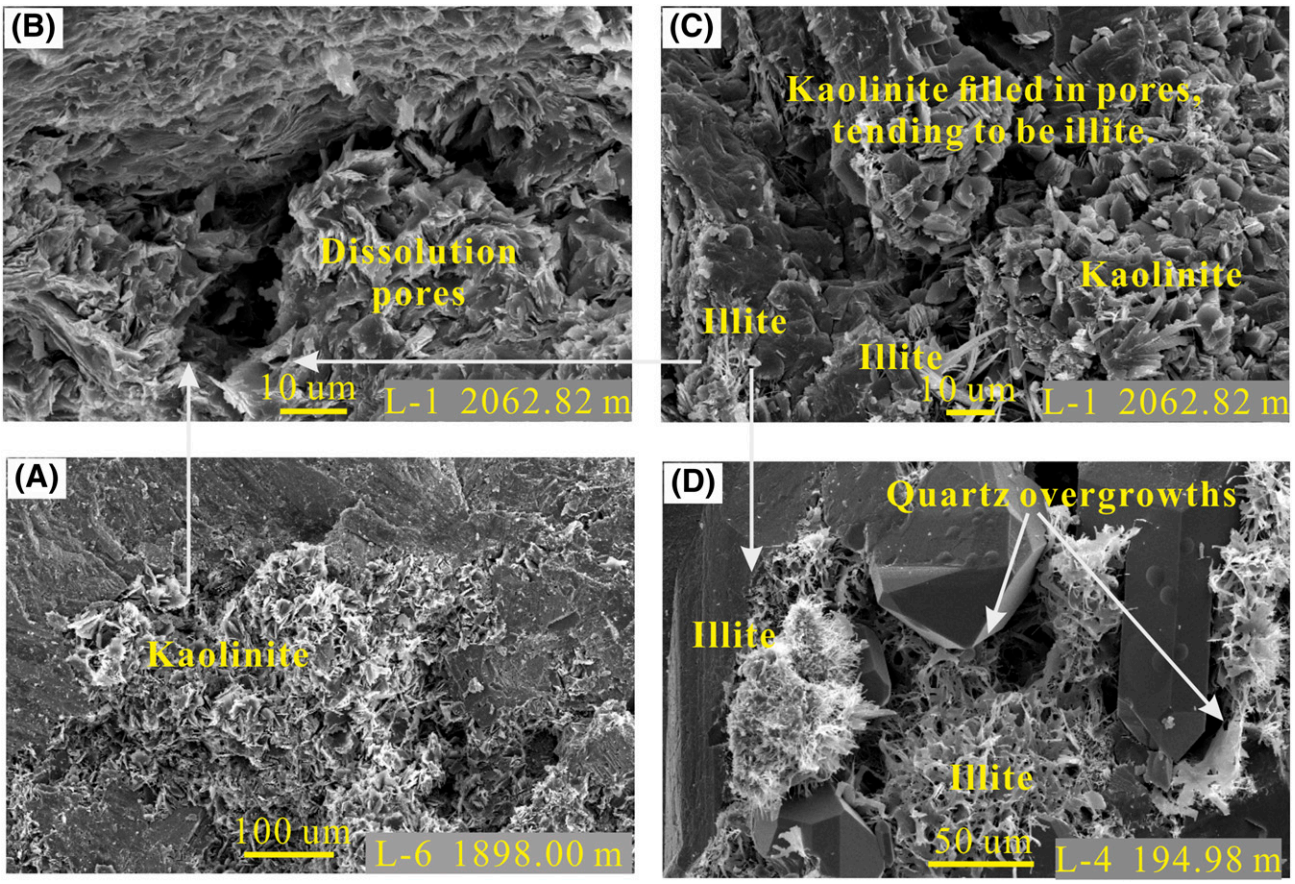

Figure 14. Influence of clay minerals on pore structure development in the Taiyuan Formation. (A) Platy kaolinite fills in the intergranular pores and intercrystalline pores developed; (B) the kaolinite is dissolved with more developed pores; (C) part of the kaolinite tends to be illite, and the transformation is in an initial stage; (D) hairlike illite infilling the pore with an overgrowth of quartz and quite limited pore spaces and the illite showing a honeycomb structure (transformed from smectite). L = well name.

temperatures greater than 120°C (Hendry et al., 2000) and participate in mesogenetic processes (Figure 15). What cannot be neglected is the effect of dissolution, with the Benxi and Taiyuan Formations having sandstones with quartz grains that are actively dissolved, resulting in a slightly increased permeability of the Taiyuan Formation. However, the porosity of the Benxi Formation does not show as large an increase as that in the Taiyuan Formation, which may be because of the greater effect of compaction and higher contents of kaolinite and illite (47% and 36%, respectively, from the XRD data in Table 3).

Key Clay Minerals Associated Different Diagenetic Process

The diagenetic evolution of the strata together with its correlation with resulting pore structure was restored (Figure 16) from thin sections, SEM images the distribution and structural relationships of the diagenetic authigenic minerals and data on sedimentary burial history. From this analysis, it is clear that the eodiagenesis process includes compaction, the development of smectite, the development of chlorite rims, the precipitation of subhedral microquartz and pore-filling authigenic quartz, the crystallization of disordered kaolinite, and precipitation of calcite and Fe-calcite. The mesogenesis process includes compaction, the precipitation of dolomite and ankerite, the precipitation of quartz cements (i.e., pore-filling amygdaloidal-shaped quartz and quartz overgrowths), the precipitation of ordered kaolinite and kaolinite to dickite transformations, the partial dissolution and replacement of feldspar, and smectite-to-illite reactions.

(A)

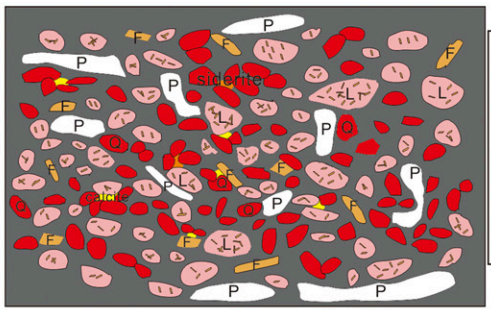

Compaction effect:

Quartz (red),debris (pink) and feldspars(light orange) compacted as a solid sedimentary rock by pressure from overlying strata; the siderite (orange) and carbonate (yellow) show an effect of cementation.

Pores are mainly of intergranular pores (white).

(B)

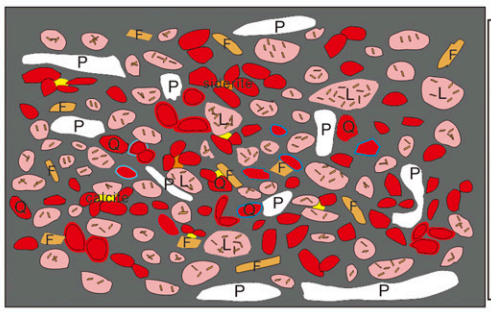

Quartz overgrowth of first stage, chlorite film occurred:

As the burial depth increases, the compaction effect increases and the volcanic debris and mica are being dissolved and first enlargement of quartz happened. Part of the quartz is surrounded by the film shaped chlorite (blue) formed by the dissolution of iron-rich sediments, which stop the overgrowth of quartz to some extent.

Primary pores decrease due to cementation.

(C)

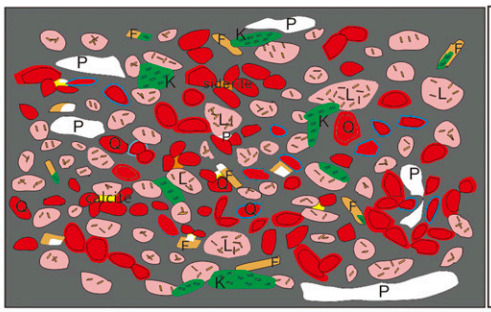

Feldspar, calcite dissolution, quartz overgrowth for the second time, authigenic kaolinite cementation:

The dissolution of feldspar and calcite accelerate the second overgrowth of quartz. The dissolved feldspar starts changing into kaolinite (green) by acidic fluid erosion,

The pore volume decreases further.

The stage can be seen in Xiashihezi and Shanxi Formations.

(D)

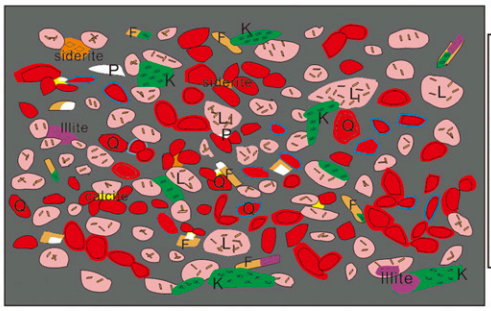

Illite, ferrocalcite and ankerite cementation:

Kaolinite transformed into smectite and illite (purple), which makes the composition of clays much more complicated.

The primary pores generally disappeared at this stage.

The stage can be seen in Shanxi and Taiyuan Formations.

(E)

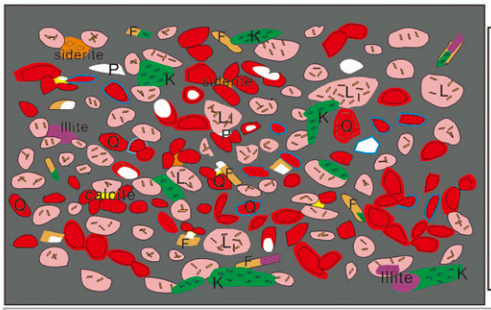

Higher degree of dissolution, with quartz dissolution:

As the temperature and pressure increases, the quartz started to be dissolved, and part of the dissolution along debris contact joints.

The pore volume shows a kind of increase.

The stage mainly happened in Taiyuan Formation.

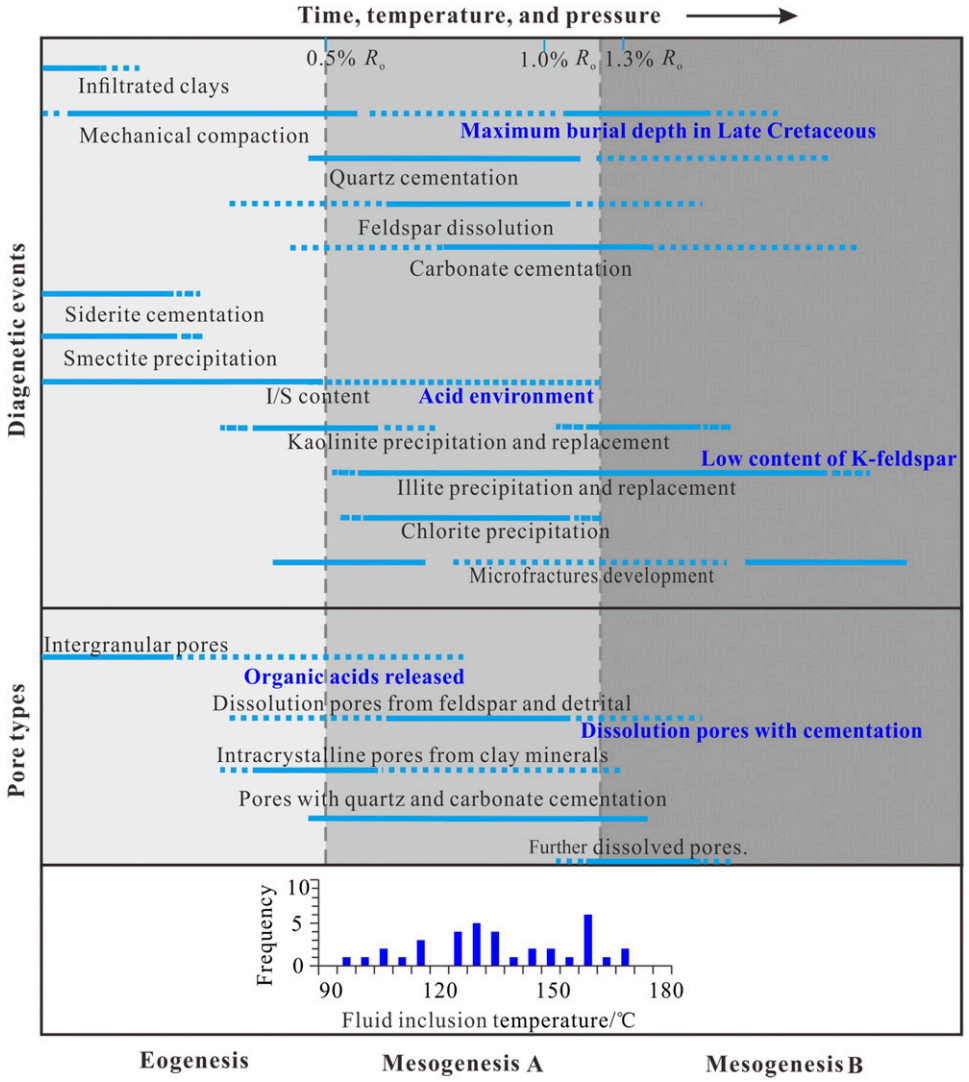

Figure 16. Paragenetic sequence and pore evolution deduced from the paragenetic relationship in tight sandstones from all the studied wells. Solid blue lines represent probable timing based on observed diagenetic and mineralization phases. Dashed blue lines represent inferred or or not well-constrained diagenetic and mineralization phases. I/S = illite–smectite; R_o = vitrinite reflectance.

The Influence of Depositional Environment on Diagenetic Process

The diageneses of strata vary by sedimentary environments (Lai et al., 2015; Vincent et al., 2015). The environments can be divided into fresh-to-semibrackish and acidic (mainly in coal-bearing strata) and alkaline waters (Vassilev et al., 2010). The upper parts of the study area represented by the Xiashihezi Formation are fluvial and consider a fresh-to-semibrackish

Figure 15. A generalized model for the evolution of minerals and pores observed in the tight sandstones. (A) Quartz, lithic fragments, and feldspars compacted by overlying strata, and pores are primarily intergranular pores; (B) volcanic debris and mica begin to be dissolved and release siliceous material to form quartz secondary enlargements. Chlorite rims occur around quartz grains during the stage, which stop the overgrowth of quartz to some degree. Intergranular pores decrease gradually because of lasting compaction and cementation; (C) further dissolution on feldspar accelerates the second quartz overgrowth. Volcanic debris and feldspar are partially replaced by kaolinite, and the pores decrease significantly; (D) kaolinite transformed into smectite and illite, and the original pores have almost disappeared; (E) quartz begins to be dissolved, and the dissolution pores increase, which turns out to be the present phenomenon.

environment. However, the coal-bearing strata from the Benxi Formation to the base of the Shanxi Formation belong to an acidic water environment.

Kaolinite is mainly derived from feldspar, and the transformation of kaolinite to illite cannot proceed in the absence of potassium ions because the present K-feldspar content is low for all the formations (Table 2). The kaolinite contents are lowest in the Taiyuan Formation in contrast to the high illite content (Figure 17B). The presence of grain-coating illite, with hairlike and honeycomblike crystals with spiny terminations, indicates a diagenetic origin through the transformation of depositional or infiltrated clays (Figure 14D; Morad et al., 2000). The increased content of illite is from the Xiashihezi to the Shanxi and Taiyuan Formations and is partly dominated by the I/S transformations, as indicated by the converse trend of I/S and kaolinite contents (Figure 17B). Furthermore, the illitization process requires a source of potassium, which in this case is probably supplied from the alteration of feldspars as apparent from the decreasing K-feldspar contents (Figure 17A; Ehrenberg, 1993; Morad et al., 2000). By inference, the alteration of feldspar, generation of illite, and creation of secondary pores may have been coincident, which would partly explain the relatively high porosity of the Taiyuan Formation sandstones (Figure 17C, D).

The average kaolinite content is especially high in the Benxi Formation (47% of all the clay minerals) because of the (1) feldspar alteration resulting from the influx of organic-derived CO_2 (Rahman and Worden, 2016) as the Benxi Formation is deposited as thin coal seams and high-organic carbonaceous mudstones (Li et al., 2016); (2) unstable illite and chlorite in an acidic environment that is converted into stable kaolinite; and (3) reality that the Benxi Formation was deposited directly on the weathering crust over approximately 130 m.y. from the Late Ordovician to early Carboniferous (Yang et al., 2005), with more weathered rock fragments transformed into kaolinite (Figure 17B; Table 3).

During the transformation of smectite to illite and congruent with pressure solution at stylolites, large quantities of silica were provided for quartz overgrowths (e.g., Figure 9B). These would promote the development of authigenic quartz overgrowths (decreasing porosity and permeability) in the Shanxi and Taiyuan Formations (Xi et al., 2015b; Ma et al., 2017). As the environment transformed from fluvial (Xiashihezi Formation) to deltaic (Shanxi Formation) and then to epicontinental (Taiyuan and Benxi Formations), the dissolution effects gradually increased. As a result, the Shanxi Formation would have mainly experienced feldspar dissolution, with the Benxi and Taiyuan Formations developing quartz dissolution pores (Figure 7J). Furthermore, the decrease in chlorite and the I/S layers is also controlled by the acids that are generated during coalification and the gas generation process (Figure 17B).

CONCLUSIONS

1. As the environment transformed from fluvial (Xiashihezi Formation) to deltaic (Shanxi Formation) and then to epicontinental (Taiyuan and Benxi Formations), dissolution effects monotonically increased. Congruent with this transition are observations that the Shanxi Formation mainly contains feldspar dissolution pores, whereas the Benxi and Taiyuan Formations contain

Table 3. Distribution of Clay Minerals from X-Ray Diffraction Data

		Clay Mineral Content, %						
Sample Nos.	Formation	Kaolinite	Illite	Chlorite	I/S	C/S	I of I/S	C of C/S
241	P_2x	23	20	29	24	4	70	19
41	P_1s	20	50	18	11	0	54	5
104	C_2t	13	78	4	5	0	17	1
18	C_2b	47	36	8	8	0	61	0

Abbreviations: C of C/S = chlorite content of chlorite/smectite; C/S = chlorite/smectite mixed layer; C_2b = Benxi Formation; C_2t = Taiyuan Formation; I of I/S = illite content of illite–smectite; I/S = illite–smectite mixed layer; Nos. = numbers; P_1s = Shanxi Formation; P_2x = Xiashihezi Formation.

Table 4. The Pores Recognized from the Section Photographs

Formations	Intergranular Pores, %	Dissolved Intergranular Pores, %	Dissolved Particle Pores, %	Dissolved Cementation Pores, %	Plane Porosity, %
Xiashihezi	0.83	1.26	1.29	0.44	3.82
Shanxi	0.13	0.69	1.71	0.54	3.07
Taiyuan	0.26	1.56	1.87	0.55	4.23
Benxi	0.16	1.63	0.63	0.68	3.11

The pores of different types were summed over the entire volume.

quartz dissolution pores. The feldspars and grain cements are partly transformed into kaolinite and are broadly distributed together with euhedral quartz overgrowths, which substantially decrease the porosity in the Shanxi Formation.

2. The eodiagenetic process includes compaction, the development of smectite, the precipitation of subhedral microquartz and associated pore filling by authigenic quartz, the crystallization of disordered kaolinite, and the precipitation of calcite and Fe-calcite. Mesogenesis includes the precipitation of dolomite and ankerite, quartz cementation, the dissolution and replacement of feldspar, and smectite-to-illite reactions.
3. The Xiashihezi Formation shows homogeneously distributed illite, chlorite, I/S, and chlorite, with the smectite and chlorite transformed from volcanic debris, sedimentary rocks, and micas altered into chlorite. The smectite appears mainly in the form of I/S mixed layers and decreases as depth increases with a transformation into honeycomb and sheet illite in the Shanxi, Taiyuan, and Benxi Formations. Because the K-feldspar content was limited with insufficient potassium ions being supplied, the transformation of kaolinite to illite was interrupted, resulting in higher contents of kaolinite in the Taiyuan and Benxi Formations.
4. The Xiashihezi Formation experienced relatively weak compaction and dissolution effects, largely retaining the original intergranular pores and developing additional dissolved intergranular pores. The Shanxi Formation commonly exhibits quartz overgrowths, with widely distributed and well-developed feldspar dissolution pores. The Taiyuan Formation has a higher porosity than the overlying sandstones in the Shanxi Formation, mainly caused by the higher content of solid quartz and the relatively strong dissolution effect. The Benxi Formation shows the lowest porosity, mainly because of the higher clay content.

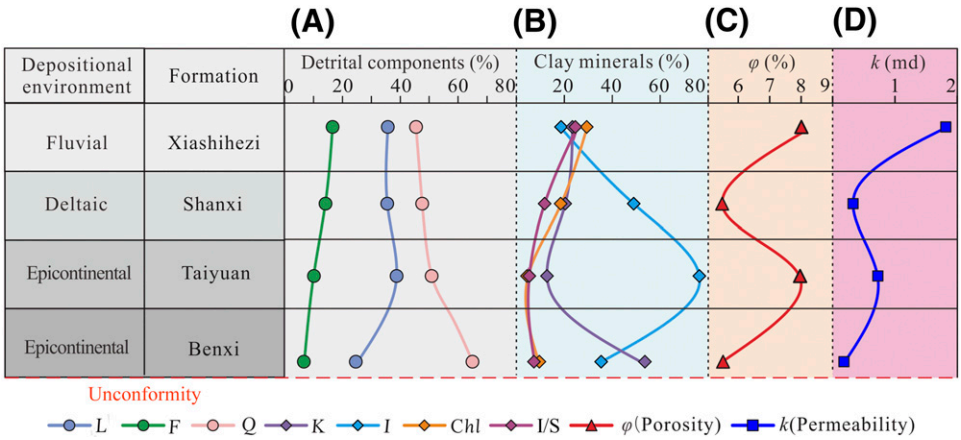

Figure 17. Average values of sandstone compositions and physical parameters of different formations. (A) Rock compositions; (B) clay mineral compositions; (C) porosity variations; (D) permeability variations. Chl = chlorite; F = feldspar; I = illite; I/S = illite–smectite mixed layer; K = kaolinite; L = lithic fragments; Q = quartz.

REFERENCES CITED

Adebayo, A. R., M. E. Kandil, T. M. Okasha, and M. L. Sanni, 2017, Measurements of electrical resistivity, NMR pore size and distribution, and x-ray CT-scan for performance evaluation of CO_2 injection in carbonate rocks: A pilot study: International Journal of Greenhouse Gas Control, v. 63, p. 1–11, doi:10.1016/j.ijggc.2017.04.016.

Al-Ramadan, K., S. Morad, J. N. Proust, and I. Al-Aasm, 2005, Distribution of diagenetic alterations in siliciclastic shorface deposits within a sequence stratigraphic framework: Evidence from the Upper Jurassic, Boulonnais, NW France: Journal of Sedimentary Research, v. 75, no. 5, p. 943–959, doi:10.2110/jsr.2005.072.

Bjørlykke, K., 2014, Relationships between depositional environments, burial history and rock properties. Some principal aspects of diagenetic process in sedimentary basins: Sedimentary Geology, v. 301, p. 1–14, doi:10.1016/j.sedgeo.2013.12.002.

Bjørlykke, K., and J. Jahren, 2012, Open or closed geochemical systems during diagenesis in sedimentary basins: Constraints on mass transfer during diagenesis and the prediction of porosity in sandstone and carbonate reservoirs: AAPG Bulletin, v. 96, no. 12, p. 2193–2214, doi:10.1306/04301211139.

Boles, J. R., and S. G. Franks, 1979, Clay diagenesis in Wilcox sandstones of southwest Texas: Implications of smectite diagenesis on sandstone cementation: Journal of Sedimentary Petrology, v. 49, p. 55–70, doi:10.1306/212F76BC-2B24-11D7-8648000102C1865D.

Cao, Z., G. Liu, W. Meng, P. Wang, and C. Yang, 2018, Origin of the different chlorite occurrences and their effects on tight clastic reservoir porosity: Journal of Petroleum Science Engineering, v. 160, p. 384–392, doi:10.1016/j.petrol.2017.10.080.

Curtis, C. D., C. R. Hughes, J. A. Whiteman, and C. K. Whittle, 1985, Compositional variation within some sedimentary chlorites and some comments on their origin: Mineralogical Magazine, v. 49, no. 352, p. 375–386, doi:10.1180/minmag.1985.049.352.08.

de Melo, M. S., G. B. Guimarães, A. L. Chinelatto, P. C. F. Giannini, H. S. Pontes, A. S. A. Chinelatto, and D. Atencio, 2015, Kaolinite, illite and quartz dissolution in the karstification of Paleozoic sandstones of the Furnas Formation, Paraná Basin, Southern Brazil: Journal of South American Earth Sciences, v. 63, no. 3, p. 20–35, doi:10.1016/j.jsames.2015.06.011.

Ece, O. I., B. Ekinci, P. A. Schroeder, D. Crowe, and F. Esenli, 2013, Origin of the Düvertepe kaolin–alunite deposits in Simav Graben, Turkey: Timing and styles of hydrothermal mineralization: Journal of Volcanology and Geothermal Research, v. 255, p. 57–78, doi:10.1016/j.jvolgeores.2013.01.012.

Ehrenberg, S. N., 1993, Preservation of anomalously high porosity in deeply buried sandstones by grain-coating chlorite: Examples from the Norwegian continental shelf: AAPG Bulletin, v. 77, no. 7, p. 1260–1286, doi:10.1306/BDFF8E5C-1718-11D7-8645000102C1865D.

El-ghali, M. A. K., H. Mansurbeg, S. Morad, I. Al-Aasm, and G. Ajdanlisky, 2006, Distribution of diagenetic alterations in fluvial and paralic deposits within sequence stratigraphic framework: Evidence from the Petrohan Terrigenous Group and the Svidol Formation, Lower Triassic, NW Bulgaria: Sedimentary Geology, v. 190, no. 1–4, p. 299–321, doi:10.1016/j.sedgeo.2006.05.021.

Fisher, Q. J., M. Casey, M. B. Clenell, and R. J. Knipe, 1999, Mechanical compaction of deeply buried sandstones of the North Sea: Marine and Petroleum Geology, v. 16, no. 7, p. 605–618, doi:10.1016/S0264-8172(99)00044-6.

Folk, R. L., 1974, Petrology of sedimentary rocks: Austin, Texas, Hemphill Publishing, 720 p.

Folk, R. L., P. B. Andrews, and D. W. Lewis, 1970, Detrital sedimentary rock classification and nomenclature for use in New Zealand: New Zealand Journal of Geology and Geophysics, v. 13, no. 4, p. 937–968, doi:10.1080/00288306.1970.10418211.

Gao, F., Y.-J. Wang, S.-S. Liu, and B.-Q. Hu, 2000, Study on thermal history of the western edge of the Ordos Basin using apatite fission tracks [in Chinese]: Geotectonica Et Metallogenia, v. 83, p. 87–91, doi:10.16539/j.ddgzyckx.2000.01.014.

Gao, X., Y. Wang, X. Ni, Y. Li, X. Wu, S. Zhao, and Y. Yu, 2018, Recovery of tectonic traces and its influence on coalbed methane reservoirs: A case study in the Linxing area, eastern Ordos Basin, China: Journal of Natural Gas Science and Engineering, v. 56, p. 414–427, doi:10.1016/j.jngse.2018.06.029.

Gier, S., R. H. Worden, W. D. Johns, and H. Kurzweil, 2008, Diagenesis and reservoir quality of Miocene sandstones in the Vienna Basin, Austria: Marine and Petroleum Geology, v. 25, no. 8, p. 681–695, doi:10.1016/j.marpetgeo.2008.06.001.

Gould, K., 2007, Chlorite diagenesis in reservoir sandstones of the Lower Missisauga Formation, offshore Nova Scotia, Master's thesis, Saint Mary's University, Halifax, Nova Scotia, Canada, 177 p.

Hakimi, M. H., M. R. Shalaby, and W. H. Abdullah, 2012, Diagenetic characteristics and reservoir quality of the Lower Cretaceous Biyadh sandstones at Kharir oilfield in the western central Masila Basin, Yemen: Journal of Asian Earth Sciences, v. 51, no. 12, p. 109–120, doi:10.1016/j.jseaes.2012.03.004.

Hakimi, M. H., M. R. Shalaby, and W. H. Abdullah, 2013, Corrigendum to "Diagenetic characteristics and reservoir quality of the Lower Cretaceous Biyadh sandstones at Kharir oilfield in the western central Masila Basin, Yemen" [J. Asian Earth Sci. 51 (2012) 109–120]: Journal of Asian Earth Sciences, v. 66, p. 295, doi:10.1016/j.jseaes.2013.02.001.

Hansen, H. N., K. Løvstad, R. Müller, and J. Jahren, 2017, Clay coating preserving high porosities in deeply buried intervals of the Stø Formation: Marine and Petroleum Geology, v. 88, p. 648–658, doi:10.1016/j.marpetgeo.2017.09.011.

Hendry, J. P., M. Wilkinson, A. E. Fallick, and N. H. Trewin, 2000, Disseminated 'jigsaw-piece' dolomite in Upper

Jurassic shelf sandstones, Central North Sea: An example of cement growth during bioturbation?: Sedimentology, v. 47, no. 3, p. 631–644, doi:10.1046/j.1365-3091.2000.00319.x.

Iijima, A., and R. Matsumato, 1982, Berthierine and chamosite in coal measures of Japan: Clays and Clay Minerals, v. 30, no. 4, p. 264–274, doi:10.1346/CCMN.1982.0300403.

Jansa, L. F., and H. N. Urrea, 1990, Geology and diagenetic history of overpressured sandstone reservoirs, Venture Gas Field, offshore Nova Scotia, Canada: AAPG Bulletin, v. 74, no. 10, p. 1640–1658.

Ji, L.-M., K. Yan, F.-W. Meng, and M. Zhao, 2010, The oleaginous Botryococcus from the Triassic Yanchang Formation in Ordos Basin, Northwestern China: Morphology and its paleoenvironmental significance: Journal of Asian Earth Sciences, v. 38, no. 5, p. 175–185, doi:10.1016/j.jseaes.2009.12.010.

Karim, A., G. Pe-Piper, and D. J. W. Piper, 2010, Controls on diagenesis of Lower Cretaceous reservoir sandstones in the western Sable Subbasin, offshore Nova Scotia: Sedimentary Geology, v. 224, no. 1–4, p. 65–83, doi:10.1016/j.sedgeo.2009.12.010.

Kordi, M., B. Turner, and A. M. K. Salem, 2011, Linking diagenesis to sequence stratigraphy in fluvial and shallow marine sandstones: Evidence from the Cambrain-Ordovician lower sandstone unit in southwestern Sinai, Egypt: Marine and Petroleum Geology, v. 28, no. 8, p. 1554–1571, doi:10.1016/j.marpetgeo.2011.05.003.

Lai, J., G. Wang, Y. Chai, Y. Xin, Q. Wu, X. Zhang, and Y. Sun, 2017, Deep burial diagenesis and reservoir quality evolution of high-temperature, high-pressure sandstones: Examples from Lower Cretaceous Bashijiqike Formation in Keshen area, Kuqa depression, Tarim basin of China: AAPG Bulletin, v. 101, no. 6, p. 829–862, doi:10.1306/08231614008.

Lai, J., G. Wang, Y. Ran, and Z. Zhou, 2015, Predictive distribution of high-quality reservoirs of tight gas sandstones by linking diagenesis to depositional facies: Evidence from Xu-2 sandstones in the Penglai area of the central Sichuan basin, China: Journal of Natural Gas Science and Engineering, v. 23, p. 97–111, doi:10.1016/j.jngse.2015.01.026.

Lai, J., G. Wang, Y. Ran, Z. Zhou, and Y. Cui, 2016, Impact of diagenesis on the reservoir quality of tight oil sandstones: The case of upper Triassic Yanchang Formation Chang 7 oil layers in Ordos Basin, China: Journal of Petroleum Science Engineering, v. 145, p. 54–65, doi:10.1016/j.petrol.2016.03.009.

Lan, C., M. Yang, and Y. Zhang, 2016, Impact of sequence stratigraphy, depositional facies and diagenesis on reservoir quality: A case study on the Pennsylvanian Taiyuan sandstones, northeastern Ordos Basin, China: Marine and Petroleum Geology, v. 69, p. 216–230, doi:10.1016/j.marpetgeo.2015.09.009.

Li, Y., D. Cao, P. Wu, X. Niu, and Y. Zhang, 2017a, Variation in maceral composition and gas content with vitrinite reflectance in bituminous coal of the eastern Ordos basin, China: Journal of Petroleum Science Engineering, v. 149, p. 114–125, doi:10.1016/j.petrol.2016.10.018.

Li, Y., D. Tang, P. Wu, X. Niu, K. Wang, P. Qiao, and Z. Wang, 2016, Continuous unconventional natural gas accumulations of Carboniferous-Permian coal-bearing strata in the Linxing area, northeastern Ordos basin, China: Journal of Natural Gas Science and Engineering, v. 36, p. 314–327, doi:10.1016/j.jngse.2016.10.037.

Li, Y., D. Tang, H. Xu, D. Elsworth, and Y. Meng, 2015, Geological and hydrological controls on water coproduced with coalbed methane in Liulin, eastern Ordos basin, China: AAPG Bulletin, v. 99, no. 2, p. 207–229, doi:10.1306/07211413147.

Li, Y., Z. Wang, Z. Pan, X. Niu, Y. Yu, and S. Meng, 2019, Pore structure and its fractal dimensions of transitional shale: A cross section from east margin of the Ordos Basin, China: Fuel, v. 241, p. 417–431, doi:10.1016/j.fuel.2018.12.066.

Li, Y., C. Zhang, D. Tang, Q. Gan, X. Niu, K. Wang, and R. Shen, 2017b, Coal pore size distributions controlled by the coalification process: An experimental study of coals from the Junggar, Ordos and Qinshui basins in China: Fuel, v. 206, p. 352–363, doi:10.1016/j.fuel.2017.06.028.

Liu, C., H. Zhao, and Y. Sun, 2009, Tectonic background of Ordos Basin and its controlling role for basin evolution and energy mineral deposits: Energy Exploration & Exploitation, v. 27, no. 1, p. 15–27, doi:10.1260/014459809788708219.

Liu, D., Y. Yao, D. Tang, S. Tang, Y. Che, and W. Huang, 2009, Coal reservoir characteristics and coalbed methane resource assessment in Huainan and Huaibei coalfields, southern North China: International Journal of Coal Geology, v. 79, no. 3, p. 97–112, doi:10.1016/j.coal.2009.05.001.

Liu, J., K. Liu, and X. Huang, 2016, Effect of sedimentary heterogeneities on hydrocarbon accumulations in the Permian Shanxi Formation, Ordos Basin, China: Insight from an integrated stratigraphic forward and petroleum system modelling: Marine and Petroleum Geology, v. 76, p. 412–431, doi:10.1016/j.marpetgeo.2016.05.028.

Liu, M., Z. Liu, J. Liu, W. Zhu, Y. Huang, and X. Yao, 2014, Coupling relationship between sandstone reservoir densification and hydrocarbon accumulation: A case from the Yanchang Formation of the Xifeng and Ansai areas, Ordos Basin: Petroleum Exploration and Development, v. 41, no. 2, p. 185–192, doi:10.1016/S1876-3804(14)60021-5.

Lundegard, P. D., 1992, Sandstone porosity loss; a "big picture" view of the importance of compaction: Journal of Sedimentary Research, v. 62, no. 2, p. 250–260, doi:10.1306/D42678D4-2B26-11D7-8648000102C1865D.

Lv, C., W.-H. Huang, and L. Fei, 2017, The provenance analysis of the 8th member of the Upper Paleozoic Shihezi Formation in the western area of Ordos Basin: Energy Sources. Part A, Recovery, Utilization, and Environmental Effects, v. 39, no. 17, p. 1886–1893, doi:10.1080/15567036.2017.1381786.

Lv, D., D. Wang, Z. Li, H. Liu, and Y. Li, 2017, Depositional environment, sequence stratigraphy and sedimentary

mineralization mechanism in the coal bed- and oil shale-bearing succession: A case from the Paleogene Huangxian Basin of China: Journal of Petroleum Science Engineering, v. 148, p. 32–51, doi:10.1016/j.petrol.2016.09.028.

Ma, B., Y. Cao, and Y. Jia, 2017, Feldspar dissolution with implications for reservoir quality in tight gas sandstones: Evidence from the Eocene Es4 interval, Dongying Depression, Bohai Bay Basin, China: Journal of Petroleum Science Engineering, v. 150, p. 74–84, doi:10.1016/j.petrol.2016.11.026.

Ma, P., C. Lin, S. Zhang, C. Dong, Y. Zhao, D. Dong, K. Shehzad, M. Awais, D. Guo, and X. Mu, 2018, Diagenetic history and reservoir quality of tight sandstones: A case study from Shiqianfeng sandstones in upper Permian of Dongpu Depression, Bohai Bay Basin, eastern China: Marine and Petroleum Geology, v. 89, p. 280–299, doi:10.1016/j.marpetgeo.2017.09.029.

Macaulay, C. I., R. S. Haszeldine, and A. E. Fallick, 1993, Distribution, chemistry, isotopic composition and origin of diagenetic carbonates: Magnus Sandstone, North Sea: Journal of Sedimentary Research, v. 63, p. 33–43, doi:10.1306/D4267A82-2B26-11D7-8648000102C1865D.

Mansurbeg, H., S. Morad, A. Salem, R. Marfil, M. A. K. El-ghali, J. P. Nystuen, M. A. Caja, A. Amorosi, D. Garcia, and A. La Iglesia, 2008, Diagenesis and reservoir quality evolution of Palaeocene deep-water, marine sandstones, the Shetland-Faroes Basin, British continental shelf: Marine and Petroleum Geology, v. 25, no. 6, p. 514–543, doi:10.1016/j.marpetgeo.2007.07.012.

Morad, S., J. M. Ketzer, and L. F. De Ros, 2000, Spatial and temporal distribution of diagenetic alterations in siliciclastic rocks: Implications for mass transfer in sedimentary basins: Sedimentology, v. 47, p.97–120, doi:10.1046/j.1365-3091.2000.00007.x.

Paxton, S. T., J. O. Szabo, J. M. Ajdukiewicz, and R. E. Klimentidis, 2002, Construction of an intergranular volume compaction curve for evaluating and predicting compaction and porosity loss in rigid-grain sandstone reservoirs: AAPG Bulletin, v. 86, no. 12, p. 2047–2067, doi:10.1306/61EEDDFA-173E-11D7-8645000102C1865D.

Rahman, M. J. J., and R. H. Worden, 2016, Diagenesis and its impact on the reservoir quality of Miocene sandstones (Surma Group) from the Bengal Basin, Bangladesh: Marine and Petroleum Geology, v. 77, p. 898–915, doi:10.1016/j.marpetgeo.2016.07.027.

Ramm, M., 1992, Porosity-depth trends in reservoir sandstones: Theoretical models related to Jurassic sandstones offshore Norway: Marine and Petroleum Geology, v. 9, no. 5, p. 553–567, doi:10.1016/0264-8172(92)90066-N.

Ren, J., L. Zhang, J. Ezekiel, S. Ren, and S. Meng, 2014, Reservoir characteristics and productivity analysis of tight sand gas in Upper Paleozoic Ordos Basin China: Journal of Natural Gas Science and Engineering, v. 19, p. 244–250, doi:10.1016/j.jngse.2014.05.014.

Rossi, C., R. Marfil, K. Ramseyer, and A. Permanyer, 2001, Facies-related diagenesis and multiphase siderite cementation and dissolution in the reservoir sandstones of the Khatatba Formation, Egypt's Western Desert: Journal of Sedimentary Research, v. 71, no. 3, p. 459–472, doi:10.1306/2DC40955-0E47-11D7-8643000102C1865D.

Schmitt, M., C. P. Fernandes, F. G. Wolf, J. A. B. da Cunha Neto, C. P. Rahner, and V. S. S. dos Santos, 2015, Characterization of Brazilian tight gas sandstones relating permeability and angstrom-to micron-scale pore structures: Journal of Natural Gas Science and Engineering, v. 27, no. 2, p. 785–807, doi:10.1016/j.jngse.2015.09.027.

Shuai, Y., S. Zhang, Y. Gao, H. Lu, J. Chen, J. Mi, J. Liu, and G. Hu, 2013, Effect and quantitative evaluation of CO_2 derived from organic matter in coal on the formation of tight sandstone reservoirs: Science China: Earth Sciences, v. 56, no. 5, p. 756–762, doi:10.1007/s11430-012-4565-2.

Stroker, T. M., N. B. Harris, W. C. Elliott, and J. M. Wampler, 2013, Diagenesis of a tight gas sand reservoir: Upper Cretaceous Mesaverde Group, Piceance Basin, Colorado: Marine and Petroleum Geology, v. 40, no. 1, p. 48–68, doi:10.1016/j.marpetgeo.2012.08.003.

Tang, S., S. Sun, D. Hao, and D. Tang, 2004, Coalbed methane-bearing characteristics and reservoir physical properties of principal target areas in North China: Acta Geologica Sinica, v. 78, p. 724–728, doi:10.3321/j.issn:1000-9515.2004.03.015.

Taylor, T. R., M. R. Giles, L. A. Hathon, T. N. Diggs, N. R. Braunsdorf, G. V. Birbiglia, M. G. Kittridge, C. I. Macaulay, and I. S. Espejo, 2010, Sandstone diagenesis and reservoir quality prediction: Models, myths, and reality: AAPG Bulletin, v. 94, no. 8, p. 1093–1132, doi:10.1306/04211009123.

Van Keer, I. P., P. Muchez, and W. Viaene, 1998, Clay mineralogical variations and evolutions in sandstone sequences near a coal seam and shales in the Westphalian of the Campine Basin (NE Belgium): Clay Minerals, v. 33, no. 1, p. 159–169, doi:10.1180/000985598545345.

Vassilev, S. V., C. G. Vassileva, D. Baxter, and L. K. Andersen, 2010, Relationships between chemical and mineral composition of coal and their potential applications as genetic indicators. Part 2. Mineral classes, groups and species: Geologica Balcanica, v. 39, p. 43–67.

Vincent, B., F. S. P. van Buchem, L. G. Bulot, M. Jaladi, R. Swennen, A. S. Hosseini, and D. Baghbani, 2015, Depositional sequences, diagenesis and structural control of the Albian to Turonian carbonate platform systems in coastal Fars (SW Iran): Marine and Petroleum Geology, v. 63, p. 46–67, doi:10.1016/j.marpetgeo.2015.02.018.

Wang, G., X. Chang, W. Yin, Y. Li, and T. Song, 2017, Impact of diagenesis on reservoir quality and heterogeneity of the Upper Triassic Chang 8 tight oil sandstones in the Zhenjing area, Ordos Basin, China: Marine and Petroleum Geology, v. 83, p. 84–96, doi:10.1016/j.marpetgeo.2017.03.008.

Wang, J., L. Feng, M. Steve, X. Tang, T. E. Gail, and H. Mikael, 2015, China's unconventional oil: A review of its resources and outlook for long-term production: Energy, v. 82, p. 31–42, doi:10.1016/j.energy.2014.12.042.

Wang, R., M. Chen, and W. Sun, 2008, Study on microscopic pore structure characteristics of ultra-low permeability sandstone reservoirs in Yanchang Formation of Ordos

Basin [in Chinese]: Geological Review, v. 54, p. 270–276, doi:10.16509/j.georeview.2008.02.014.

Worden, R. H., and S. Morad, eds., 2009, Clay mineral cement in sandstones: Hoboken, New Jersey, John Wiley & Sons, 520 p.

Worden, R. H., P. C. Smalley, and S. A. Barclay, 2003, H_2S and diagenetic pyrite in North Sea sandstones: Due to TSR or organic sulphur compound cracking?: Journal of Geochemical Exploration, v. 78–79, p. 487–491, doi:10.1016/S0375-6742(03)00072-4.

Xi, K., Y. Cao, J. Jahren, R. Zhu, K. Bjørlykke, B. G. Haile, L. Zheng, and H. Hellevang, 2015a, Diagenesis and reservoir quality of the lower Cretaceous Quantou Formation tight sandstones in the southern Songliao Basin, China: Sedimentary Geology, v. 330, p. 90–107, doi:10.1016/j.sedgeo.2015.10.007.

Xi, K., Y. Cao, Y. Wang, B. G. Haile, X. Zhang, J. Zhang, and J. Jin, 2015b, Diagenesis and porosity-permeability evolution of low permeability reservoirs: A case study of Jurassic Sangonghe Formation in Block 1, central Junggar Basin, NW China: Petroleum Exploration and Development, v. 42, no. 4, p. 475–485, doi:10.1016/S1876-3804(15)30040-9.

Xu, N., L. Qiu, K. A. Eriksson, Y. I. Klyukin, Y. Wang, and Y. Yang, 2017, Influence of detrital composition on the diagenetic history of tight sandstones with implications for reservoir quality: Examples from the Permian Xiashihezi Formation and Carboniferous Taiyuan Formation, Daniudi gas field, Ordos Basin, China: Marine and Petroleum Geology, v. 88, p. 756–784, doi:10.1016/j.marpetgeo.2017.09.018.

Xu, Z., L. Liu, T. Wang, K. Wu, X. Gao, W. Dou, F. Xiao, N. Zhang, X. Song, and H. Ji, 2017, Application of fluid inclusions to the charging process of the lacustrine tight oil reservoir in the Triassic Yanchang Formation in the Ordos Basin, China: Journal of Petroleum Science Engineering, v. 149, p. 40–55, doi:10.1016/j.petrol.2016.10.014.

Yang, Y., W. Li, and L. Ma, 2005, Tectonic and stratigraphic controls of hydrocarbon systems in the Ordos basin: A multicycle cratonic basin in Central China: AAPG Bulletin, v. 89, no. 2, p. 255–269, doi:10.1306/10070404027.

Yang, Z., Q. Li, S. Wu, S. Lin, and X. Liu, 2017, Evidence of the near-source accumulation of the tight sandstone gas in northern Ordos Basin, North-Central China: Acta Geologica Sinica, v. 91, no. 5, p. 1820–1835, doi:10.1111/1755-6724.13413.

Yao, Y., D. Liu, D. Tang, S. Tang, Y. Che, and W. Huang, 2009, Preliminary evaluation of the coalbed methane production potential and its geological controls in the Weibei Coalfield, Southeastern Ordos Basin, China: International Journal of Coal Geology, v. 78, no. 1, p. 1–15, doi:10.1016/j.coal.2008.09.011.

Yasuhara, H., D. Elsworth, and A. Polak, 2003, A mechanistic model for compaction of granular aggregates moderated by pressure solution: Journal of Geophysical Research Solid Earth, v. 108, no. B11, p. 2530–2543, doi:10.1029/2003JB002536.

Yuan, G., J. Gluyas, Y. Cao, N. H. Oxtoby, Z. Jia, Y. Wang, K. Xi, and X. Li, 2015, Diagenesis and reservoir quality evolution of the Eocene sandstones in the northern Dongying Sag, Bohai Bay Basin, East China: Marine and Petroleum Geology, v. 62, p. 77–89, doi:10.1016/j.marpetgeo.2015.01.006.

Zhang, L., G. Bai, X. Luo, X. Ma, M. Chen, M. Wu, and W. Yang, 2009, Diagenetic history of tight sandstones and gas entrapment in the Yulin Gas Field in the central area of the Ordos Basin, China: Marine and Petroleum Geology, v. 26, no. 6, p. 974–989, doi:10.1016/j.marpetgeo.2008.05.003.

Zhang, Y., G. Pe-Piper, and D. J. W. Piper, 2015, How sandstone porosity and permeability vary with diagenetic minerals in the Scotian Basin, offshore eastern Canada: Implications for reservoir quality: Marine and Petroleum Geology, v. 63, p. 28–45, doi:10.1016/j.marpetgeo.2015.02.007.

Zhao, J., Y. Bai, Q. Cao, and E. Chuang, 2012, Quasi-continuous hydrocarbon accumulation: A new pattern for large tight sand oilfields in the Ordos basin: Oil and Gas Geology, v. 33, no. 6, p. 811–827, doi:10.11743/ogg20120601.

Zhu, R., C. Zou, N. Zhang, X. Wang, R. Cheng, L. Liu, C. Zhou, and L. Song, 2008, Diagenetic fluids evolution and genetic mechanism of tight sandstone gas reservoirs in Upper Triassic Xujiahe Formation in Sichuan Basin, China: Science in China Series D: Earth Sciences, v. 51, no. 9, p. 1340–1353, doi:10.1007/s11430-008-0102-8.

Zhu, S., X. Zhu, X. Liu, D. Wu, and D. Zhao, 2016, Authigenic minerals and diagenetic evolution in altered volcanic materials and their impacts on hydrocarbon reservoirs: Evidence from the lower Permian in the northwestern margin of Junggar Basin, China: Arabian Journal of Geosciences, v. 9, p. 1–19, doi:10.1007/s12517-015-2201-0.

Zou, C., G. Zhang, Z. Yang, S. Tao, L. Hou, R. Zhu, X. Yuan, Q. Ran, D. Li, and Z. Wang, 2013, Concepts, characteristics, potential and technology of unconventional hydrocarbons: On unconventional petroleum geology: Petroleum Exploration and Development, v. 40, no. 4, p. 413–428, doi:10.1016/S1876-3804(13)60053-1.